J Math Chem (2010) 47:229–267
DOI 10.1007/s10910-009-9566-9

ORIGINAL PAPER

Optimal vulcanization of 2D–3D EPM/EPDM thick elements through peroxidic mixtures

G. Milani · F. Milani

Received: 11 March 2009 / Accepted: 26 June 2009 / Published online: 17 July 2009

Abstract In the present paper, a numerical procedure for the optimal vulcanization of 2D and 3D thick rubber elements by means of peroxides mixtures is presented. When dealing with the curing process of thick EPM/EPDM items, the main problem in industrial practice is constituted by the different temperatures which undergo internal (cooler) and external regions. Indeed, while internal layers remain essentially unvulcanized, external coating is always over-vulcanized, resulting in an overall average tensile strength insufficient to permit the utilization of the items in several applications where it is required a certain level of performance. A possibility to improve rubber output mechanical properties is the utilization of mixtures of at least two peroxides, one highly active at high temperatures (i.e. for external layers), the other at lower (internal regions). In this framework, a genetic algorithm with zooming and elitist strategy is adopted for the determination of optimal input parameters to use for the production of complex 3D/2D thick items. Vulcanization external temperature T_c, rubber exposition time t and different peroxides mixtures are assumed as input production parameters, whereas output mechanical property to optimize is represented by the average tensile strength of the item. The GA approach proposed exploits a zooming-elitist strategy, consisting in the subdivision of the population at each iteration into two sub-groups, depending on individuals grade of fitness. Two meaningful examples of engineering interest, consisting of a 3D thick rubber docks bumper and an extruded (2D) relatively thick wheatear strip are illustrated, using different mixtures (50–50%, 25–75% and 75–25% molar ratios) of two peroxides. Optimal production T_c and t parameters are

G. Milani (✉)
Politecnico di Milano, Piazza Leonardo da Vinci 32, 20133 Milan, Italy
e-mail: gabriele.milani@polimi.it; milani@stru.polimi.it

F. Milani
CHEM.CO Consultant, Via J.F. Kennedy 2, 45030 Occhiobello, Rovigo, Italy
e-mail: federico-milani@libero.it

obtained for all the cases analyzed. Numerical simulations show how different mixtures of peroxides may (a) reduce optimal curing time at almost constant optimized tensile strength or (b) increase optimal tensile strength with an acceptable increase of the curing time.

Keywords EPM/EPDM elastomers · Vulcanization · Genetic algorithm · Fourier's heat transmission law

1 Introduction

EPM/EPDM elastomers are used in engineering practice in a wide range of applications, including e.g. high/medium voltage power cables insulation, weather strips, docks bumpers, etc.

An increasing penetration of EPM/EPDM into the cross-linked polyethylene (XLPE) market share is expected by the majority of producers in the next few years, due to the increasing need of utilizing polymeric items at relatively high temperatures (high voltage cables insulators, ships bumpers, dissipation energy devices for various engineering applications, including cars elements, trucks, army vehicles, etc.). As well known, XLPE hardily matches such increasing restricting requirements, due to its dimensional stability problems at temperatures above 90 °C.

On the other hand, in several cases of industrial interest, a threshold value of a-priori established rubber output mechanical properties (e.g. tensile strength, tear resistance, etc.) is required, in order to avoid premature failures and/or insufficient performance.

Unfortunately, EPM/EPDM producers are usually unable to guarantee a good and homogeneous degree of vulcanization in presence of thick rubber elements, a quite important drawback strictly connected to the fact that external rubber layers undergo temperatures profiles totally different with respect to the internal ones. This matter implies the impossibility to utilize thick rubber items in applications where it is required a high level/high quality mechanical performance of the product.

In a few literature works [1–3] the industrial vulcanization process in continuum of EPM/EPDM insulated medium and high voltage electric cables was described in detail. Nevertheless, since cables thickness does not exceed 1 cm in the most unfavourable case (i.e. medium and high voltage cables), vulcanization degree is usually optimal both for the internal and the external layers, thus reflecting in output mechanical properties of the cables adequate for guaranteeing sufficient tear and tensile strength, good elongation in the inelastic phase, good resistance to electric treeing, etc.

The overall vulcanization level prediction becomes much more complicated when thicknesses exceed generally 2 cm and dealing with complex 3D geometries.

In this framework, it appears particularly interesting from a theoretical point of view, to present a numerical model able both to (1) predict temperature profiles for each point of a generic 3D rubber item subjected to vulcanization and to (2) furnish an estimation of EPM/EPDM average mechanical properties expected at the end of the production process.

Furthermore, the determination of rubber final vulcanization degree has been inspected from a mathematical point of view only in the axi-symmetric case [1–3],

usually by means of unsophisticated numerical techniques, based on the finite differences approach.

As a consequence, at present, a model able to reproduce final rubber mechanical properties when dealing with complex 2D and 3D geometries is still lacking.

As well know, in the production process, a wide spread of commercial peroxides is used, since they ensure a defined level of vulcanization of the final product at a given curing temperature.

As already pointed out, the most important issue during the vulcanization of thick rubber items is the inhomogeneous degree of vulcanization obtained at the end of the industrial process, due to the very different temperature conditions which undergo external layers with respect to the core. Therefore, it appears particularly interesting to analyze mixtures of two peroxides able to vulcanize EPM/EPDM rubber at different temperatures, highly active the first for external layers, the second for the core. In the paper, for the sake of conciseness only a set of mixtures of 2.5-dimethyl-2.5-bis-(*t*-butylperoxy)-hexane (AkzoNobel Trigonox 101 [4] hereafter called Peroxide E) and 1.1 bis (*t*-butyl-peroxy)-3.3.5 trimetylcyclohexane (AkzoNobel Trigonox 29 [4], hereafter called Peroxide A) is considered. Such peroxides have considerable differences in $t_{1/2}$ at 6 min (0.1 h), respectively at 171 and 138 °C. Both are usually utilized in practice to vulcanize EPM/EPDM rubber and their marked different behaviour seems particularly suited to obtain a homogeneous vulcanization of thick items.

Mixing molar ratios considered are 50–50%, 75–25% and 25–75%. Results obtained with the aforementioned mixing ratios are compared with 0–100%, 100–0% mixtures, representing vulcanization with only Trigonox 101 and Trigonox 29, respectively.

Fourier's heat equation in its general 3D form is used for the determination of temperature profiles for complex rubber 3D items obtained by extrusion, compression and injection molding (see Fig. 1).

Rubber tensile strength is monitored as output quantity to optimize. Nevertheless, it is stressed that the approach proposed is aimed at selecting any output mechanical property as optimization objective function, meaning that the procedure could be used by manufactures in a general framework and without any conceptual difficulty.

It is worth noting that a fundamental parameter which enters into the optimization process, is the relation among half life of peroxides used for cross-linking process ($t_{1/2}$), temperature of each point of the item during the heating process and mechanical properties of rubber as a function of unreacted peroxide.

In particular, several questions arise from the previous aspects, related to the fact that experimental evidences show [5,6] that rubber mechanical properties (e.g. tensile strength, elongation, tear resistance, etc.) depend non-linearly on the unreacted peroxide concentration C_i. More in detail, for high values of C_i, rubber results not vulcanized with a very low tensile/tear strength, whereas for lower values of C_i, experience shows that an optimal concentration $\overline{C}_i$ exists in correspondence of which output mechanical properties reach their maximum. Further complications arise when dealing with a mixture of peroxides, for which unreacted concentrations vary differently for each peroxide at different points of the item.

Maximization of rubber final tensile strength is obtained by means of a GA approach based on a specifically crafted zooming strategy, consisting in the subdivision of the population at each iteration into two sub-groups, depending on individuals grade of

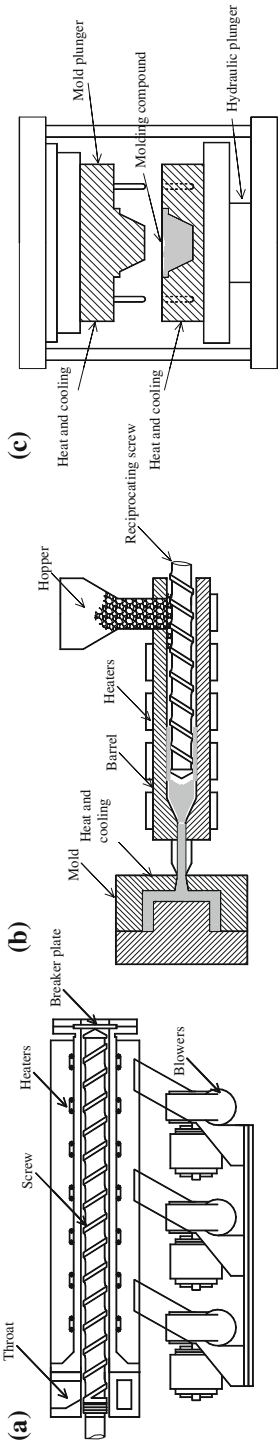

Fig. 1 Schematic representation of the vulcanization process during extrusion (**a**), injection moulding (**b**) and compression moulding (**c**)

fitness (elitist strategy). Different genetic procedures are applied to the sub-groups, consisting of both two typologies of admissible mutations for the elite sub-population and mutation and reproduction for the remaining individuals. The utilization of a non standard GA is preferable in terms of time required for the simulations with respect to a traditional subdivision of the domain into a regular grid of points.

It is worth underlining that the procedure proposed is mainly theoretical and is aimed at finding if it is possible to reduce the cross-linking time required or alternatively the temperature of vulcanization or both, in order to obtain optimized rubber mechanical properties from the surface to the core of the items.

Two meaningful examples of engineering interest, consisting of a 3D thick rubber docks bumper and an extruded (2D) relatively thick wheatear strip are illustrated at the end of the paper, using different mixtures (50–50%, 25–75% and 75–25% molar ratios) of peroxides A and E.

In both cases, optimal production T_c and t parameters are numerically evaluated. Simulations show how different mixtures of peroxides may (a) reduce optimal curing time at almost constant optimized tensile strength or (b) increase optimal tensile strength with an acceptable increase of the curing time.

2 3D rubber thick elements vulcanization

At present, vulcanization of rubber thick elements (as for instance docks bumpers or thick glass seal weather-strips) is a very difficult task, causing several technical problems to manufacturers. Usually, a theoretical approach is not taken into consideration, due to the complexity of the problem itself, with the subsequent adoption of empirical approaches. Technical problems are due to the impossibility to assure, during the vulcanization process, a homogeneous distribution of temperatures between internal (cool) zone and external (hot) boundaries. As a matter of fact, this always results in an over-vulcanization of the external coating and an insufficient curing of the internal regions of the elements.

Consequently, resultant cured elements are almost always of poor quality and, we believe, cannot have a large widespread in engineering applications.

Almost the totality of the items available in the commercial market are obtained by compression (or injection) moulding or extrusion, see Fig. 1. Manufacturing of rubber products always involves the following steps: mixing, shaping and vulcanization. In both procedures, in the mixing step, the aim is to get all ingredients dispersed homogeneously at controlled temperature. Especially the carbon black and the peroxides have to be well dispersed. The subsequent step is the final product shaping. This can be done either continuously (i.e. by extrusion), or intermittently, i.e. through some kind of moulding process. The oldest moulding technique (and still very much used), is compression moulding. The material is inserted manually into the hot mould, which is divided into two halves. Then the mould is closed and the rubber flows out into all cavities and vulcanization takes place. Transfer moulding looks almost the same, with the only exception that the material is transferred (i.e. injected) into the mould cavity from a pre-chamber. Injection moulding is the most automated moulding technique and works almost like injection moulding of thermoplastics. The rubber

material is fed into a reciprocating screw, which rotates slowly backward as the rubber is conveyed in frontal direction. Then the screw is pushed forward and the material flows through the nozzle, collecting into the hot mould. When the rubber product has vulcanized enough to be stable in shape, the mould is opened and the product ejected.

When dealing with rubber docks bumpers, vulcanization occurs almost always by means of compression (or injection) moulding, hence heat flux transmits by the steel punch to the not vulcanized rubber by conduction.

On the contrary, wheatear-strips are obtained by extrusion, hence heat flux is assured by conduction and radiation, in analogy to the production process of electric power cables insulations.

In both cases, we can schematically assume that a heating zone is followed by a cooling phase with water and/or air, as in Fig. 1. In the first phase, cross-linking of polymer is obtained by curing with increasing temperature transmitted from the boundary to each of the element by conduction or heat convection. Finally the resultant cured object is leaved and cooled in the surrounding air by free convection. With the aim of optimizing the production line, many parameters have to be chosen carefully. In particular, the following variables play a crucial role: exposition time, temperature of the heating phase and temperature of the cooling phase. As it will be shown in what follows, a simple Genetic Algorithm (GA) can be profitably applied in order to give interesting information on nitrogen temperature and exposition time of the items.

3 Vulcanization process by peroxidic reticulation

A number of different elastomers can be cross-linked using peroxides [7–13]. The utilization of peroxides is due to their easiness of formation of free radicals.

When dealing with EPM/EPDM elastomers, cross-linking occurs by means of common organic peroxides. EPM/EPDM rubber, in fact, is constituted by saturated linear macromolecules with a paraffinic structure, with controlled quantities of insaturations (for EPDM), external to the main chain.

On the other hand, from a theoretical point of view, the selection of the most appropriate peroxide is a very difficult task since it is obviously necessary to have a deep knowledge of both the application to which the peroxide is used and the process method, as well as the operating conditions to be used.

For the problem at hand, for instance, the reaction temperature (which is a function of curing temperature via partial differential equations) is the fundamental parameter on which the choice of the organic peroxide depends. In fact, it is worth noting that peroxide decomposition kinetic, which has a key role in the cross-linking mechanism, varies enormously at different temperatures. That means that each point of the object withstands different temperature histories, hence the peroxide may be less or more active during the vulcanization passing from one point to another. This is particularly evident when thick rubber elements are considered, i.e. when a production process where large differences in the temperature profiles between internal and external layers is expected.

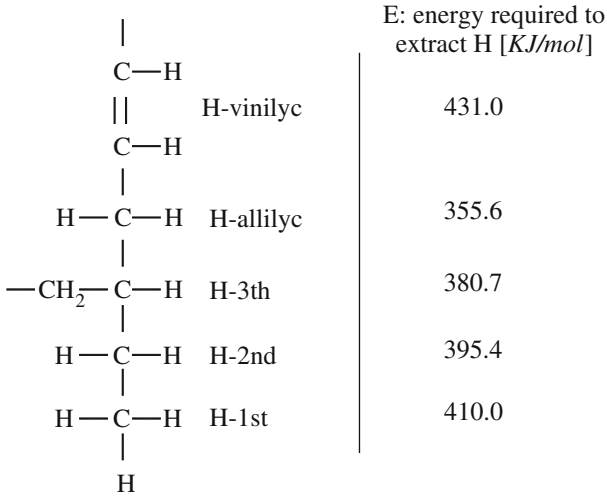

Fig. 2 Energy required to extract hydrogen atom from the backbone of the macromolecules

3.1 Vulcanization of saturated hydrocarbons elastomers through peroxides: general reticulation kinetics

Peroxides are important for rubber vulcanization, because of their ability to cross-link elastomers that contain no sites for attack by other types of vulcanization agents [14]. For EPM/EPDM, peroxides cross-linking may (a) improve throughput without loss of surface aspect, (b) provide improved head aging, (c) accept lower filler content and (d) promote the production of food-grade items. Moreover, properties of vulcanized rubber by peroxides are often very similar to radiation cross-linked materials, because both curing systems result in carbon-carbon cross-links. Furthermore, peroxides cross-linking involves formation of carbon-carbon bonds that are more stable with respect to sulphur-sulphur bonds in sulphur accelerators cross-linking [14].

The first step in a peroxide-induced vulcanization is the decomposition of the peroxide to give free radicals [15,16], i.e. peroxide $\rightarrow$ 2R$\bullet$, where R$\bullet$ is an alkoxil, an alkyl or an acyloxyl radical, depending on the typology of peroxide used.

The efficiency of the cross-linking process depends either on the difficulty (in an energetic meaning) to extract the hydrogen atom from the backbone of the macromolecules (see [17]), as show in Fig. 2, or from the reactions required to deplete the radicals [15,18].

Peroxides can also cross-link saturated hydrocarbon polymers [18], as shown in Fig. 3; in this case, the efficiency is reduced by branching.

When saturated ethylene-propylene rubbers are considered, it has been shown that the efficiency is a function of the propylene content [18–20] (Fig. 4). For a mathematical interpretation of the cross-linking process [2,21], it is needed to have at disposal formulas to use in practice able to predict kinetic decomposition of peroxides as a function of rubber composition, vulcanization conditions (temperature and exposition time) and peroxide unreacted concentration.

Fig. 3 Peroxidic vulcanization of saturated hydrocarbon elastomers

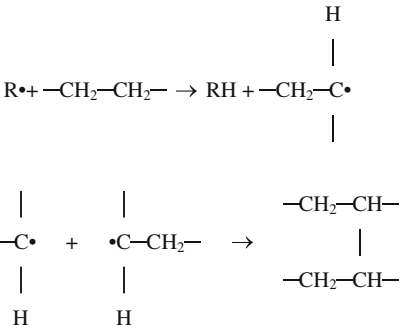

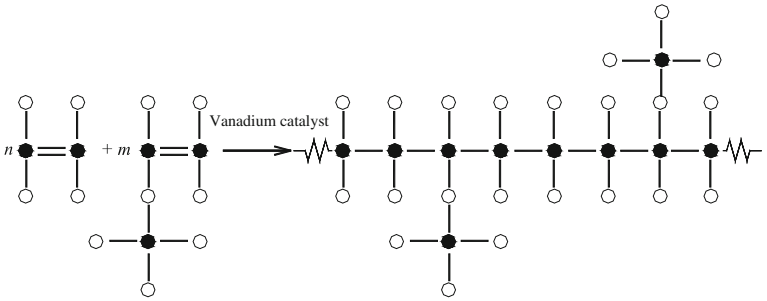

Fig. 4 Basic structure of ethylene propylene copolymers

As a rule, peroxides decomposition kinetic is of first order, i.e. $-\frac{dC}{dt} = kC$ where C is the concentration (expressed for instance in mol/m^3) of the unreacted peroxide and k is a kinetic constant for a fixed peroxide.

The analytical solution of such a differential equation can be obtained by simply splitting variables if and only if k does not depend on exposition time, leading to:

$$C(t)/C_0 = e^{-kt} \tag{1}$$

where C_0 is the initial peroxide concentration (all unreacted) and $C(t)$ is the unreacted peroxide concentration at time t. Defining as half life $t_{1/2}$ the time required to obtained a concentration of unreacted peroxide equal to $C_0/2$, Eq. 1 leads to define k as $k = \ln 2/t_{1/2}$.

Therefore, reaction kinetic law (1) can be re-written as follows:

$$\frac{C(t)}{C_0} = \frac{1}{2} e^{\left(1-\frac{t}{t_{1/2}(T)}\right)\ln 2} \tag{2}$$

This last equation describes the absolute decrease of peroxide unreacted concentration at different times with respect to parameter $t_{1/2}$.

As experimental evidences show, the rate of reaction, and hence $t_{1/2}$ (or analogously velocity constant k), are temperature dependent. In Fig. 5, for instance, the behavior at

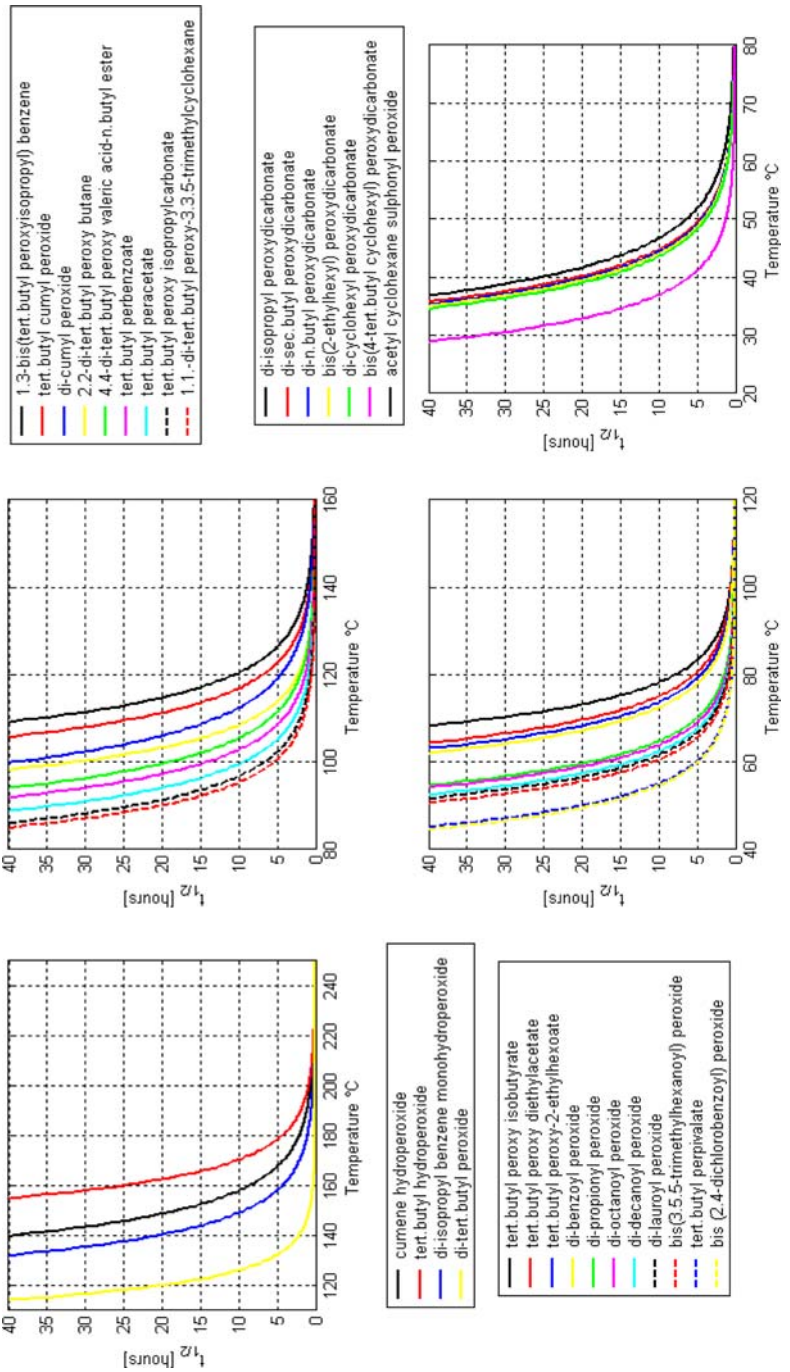

Fig. 5 Commercial peroxides temperature $t_{1/2}$ curves

different temperatures in terms of $t_{1/2}$ parameter for 32 different peroxides commonly used are reported.

As well known, such a dependence is expressed by the classical Arrhenius equation [2,13]:

$$k(T) = k_{\max} e^{-\frac{E_a}{R_g T}} \tag{3}$$

where:

- $k(T)$ is the peroxide velocity constant at a temperature T;
- E_a is the so-called energy of activation $\left[\frac{\text{kJ}}{\text{mol}}\right]$;
- R_g is the general gas constant ($8.134\left[\frac{\text{J}}{\text{molK}}\right]$);
- T is the absolute temperature;
- $k_{\max}$ is the velocity constant for $T \to +\infty$.

Form Eq. 3, it can be proved that:

$$\begin{aligned} t_{1/2}(T_2)/t_{1/2}(T_1) = e^{-\frac{E_a}{R_g}\left(\frac{1}{T_1}-\frac{1}{T_2}\right)} \Rightarrow \ln(t_{1/2}(T_2)) - \ln(t_{1/2}(T_1)) \\ = \frac{E_a}{R_g}\left(\frac{1}{T_1} - \frac{1}{T_2}\right) \end{aligned} \tag{4}$$

where T_1 and T_2 are two generic absolute temperatures.

From Eq. 4 it follows that a semi-logarithmic plot of $t_{1/2}$ half life decomposition with respect to the reciprocal of absolute temperature $1/T$ is a straight line with angular coefficient equal to $-E_a/R_g$. Law (4) is commonly used by practitioners in order to have an idea of the peroxide to use in the manufacturing process. As a rule, engineers know (from their own experience) approximately exposition time and curing temperature T_c. From exposition time, peroxide to use is normally selected multiplying exposition time by 0.3, hence finding $t_{1/2}$ half life decomposition of the plant. In this way, a restricted number of commercial peroxides are selected. Considering also that the maximum value of the temperature profile for external rubber layers is usually not far from T_c (is equal to T_c for vulcanization by conduction), manufactures experience drives the final choice of the peroxide to use.

On the other hand, when dealing with thick rubber elements, temperature field between external and internal layers remains unavoidably inhomogeneous, thus precluding a good overall vulcanization of the elements. Since internal layers remain relatively cool with respect to external coat (which tends to be over-vulcanized), it would be particularly useful to establish, by means of a numerical/theoretical model, a double-peroxide mix to use to optimize overall vulcanization. The aim is to activate vulcanization of the cool internal zone with one peroxide, whereas the other is active for the hot coat.

When a total initial concentration C_0 of two peroxides is present in the mixture, we assume that each peroxide decompose separately following a first order differential equation. Indicating with index 1 and 2 peroxide 1 and 2, respectively and with $C = C_1 + C_2$ the sum of peroxides unreacted concentrations, we obtain:

$$\begin{aligned} -\tfrac{dC_1}{dt} &= k_1 C_1 \\ -\tfrac{dC_2}{dt} &= k_2 C_2 \end{aligned} \Rightarrow -\frac{d(C_1 + C_2)}{dt} = k_1 C_1 + k_2 C_2 \tag{5}$$

Assuming that $C_{10} = \chi C_0$ and $C_{20} = (1 - \chi)C_0$ are initial peroxides concentrations and supposing that each peroxide constant k_i follows Arrhenius Equation 3, we obtain:

$$-\frac{d(C/C_0)}{dt} = \chi k_{1\max} e^{\frac{E_{a1}}{R_g T}} \frac{C_1}{C_{10}} + (1 - \chi) k_{2\max} e^{\frac{E_{a2}}{R_g T}} \frac{C_2}{C_{20}} \tag{6}$$

which gives the variation of total unreacted peroxides concentration with respect to actual concentrations of peroxides.

It is interesting to notice from Eqs. 6 and 5 that an integral may be obtained analytically only supposing temperature T constant. Obviously, during vulcanization, $T = T(t)$ and therefore a numerical integration is needed for each point of the items to vulcanize. In particular an explicit Runge–Kutta (4,5) formula [22] is utilized because it needs only the knowledge of the solution at the immediately preceding time point.

In what follows, we present a mixed Genetic Algorithm (GA) Finite Element (FEM) procedure [23] aimed at the determination of optimal input parameters (curing temperature T_c, exposition time t and peroxides mix) aimed at the optimization of the output rubber mechanical properties.

3.2 Cured rubber tensile strength

Thick rubber 3D and 2D elements are not widely diffused and produced, probably due to their typical poor mechanical properties, obvious consequence of an inhomogeneous vulcanization, which usually cannot easily be controlled by manufactures during the production process.

Vulcanized rubber and thermoplastic elastomers (TPE) often fail in service due to the generation and propagation of special type of ruptures, called “tear”, with elasto-plastic and even fragile phenomena. Other usual failures that produce enormous economical losses is those due to the lack of tensile strength, which for instance causes dangerous water infiltrations even in service conditions. From the above considerations, it appears particularly interesting to propose an optimization process able to maximize, both for 3D and 2D thick elements, tensile strength σ_t [24].

An optimization of such output parameters is possible for thick elements if a mixture of at least two peroxides is used, in order to cross-link cool parts with one peroxide and hot regions with the other.

From a theoretical and practical point of view, to link the vulcanization process with mechanical properties of rubber is not an easy task.

Experimental tests conducted on EPM/EPDM rubber using a number of different peroxides (see [6] and also [7,25]) showed that rubber macroscopic mechanical properties (tear resistance, tensile strength, Young modulus, etc.) depend on C/C_0 ratio, where C is the concentration of unreacted peroxide and C_0 is its initial concentration the mixture, see Fig. 6. Since peroxide concentration depends on curing time via half

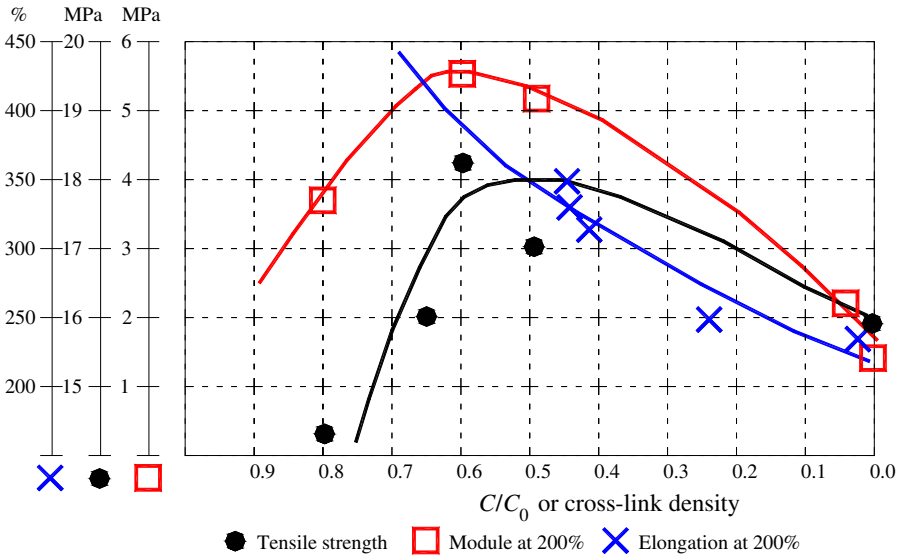

Fig. 6 Non linear behaviour of output rubber mechanical properties with respect to peroxide unreacted concentration (data processed from Hofmann experimentation [6])

life $t_{1/2}$ parameter (see Eq. 2) and remembering that $t_{1/2}$ is a function of absolute temperature T, it appears clear that rubber macroscopic mechanical properties are dependent on curing time [6] in a non trivial way.

In particular, it has been shown that tensile strength depends on unreacted peroxide concentration (or curing time) in a non monotonic way, meaning that a maximum is reached at ureacted peroxide concentrations >0.

An excess in curing time usually results in a slight decrease of final strength, as shown in Fig. 7 and by Hoffmann [6].

In an equivalent way, tensile strength may be regarded as dependent on cross-link density, being C/C_0 a measure of cross-linking, Fig. 7.

In Fig. 8, rubber behavior vulcanized with peroxide E and peroxide A is shown as a function of temperature and exposition time. In particular, in Fig. 8a and c tensile strength function is reported, whereas in Fig. 8b and d unreacted peroxide concentration is plotted as a function of T and t. As it is possible to notice, Fig. 8a and c, optimal tensile strength is reached only at particular values of T and t. Obviously, such a representation is able to give correct information on output parameters only at constant temperatures (note that $T \neq T_c$, being T rubber temperature), i.e. results reported in Fig. 8 cannot be applied directly to a rubber infinitesimal element subjected to curing, because its temperature changes continuosly at successive time steps.

As well known, in fact, real non constant temperature profiles $T = T(\mathbf{P}, t)$ for each point $\mathbf{P}$ of the element to vulcanize have to be determined solving a suitable differential system, as it will be shown in what follows. Nonetheless, Fig. 8 gives technically useful (even approximate) information on the complex behavior of rubber during vulcanization, addressing that a strong variability of output mechanical properties is obtained changing peroxide.

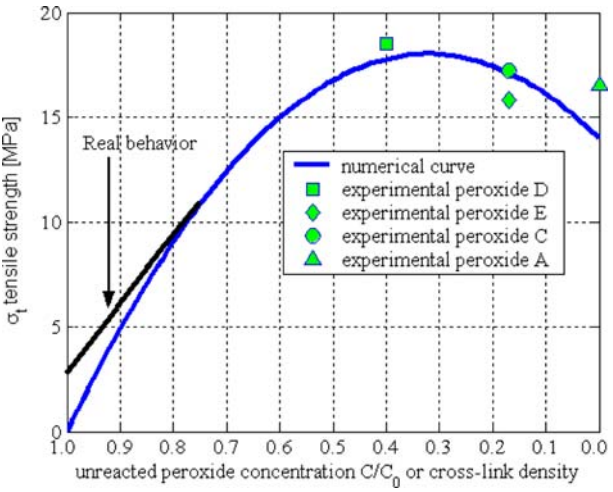

Fig. 7 Quadratic interpolation of experimental data, tensile strength-unreacted peroxide concentration data

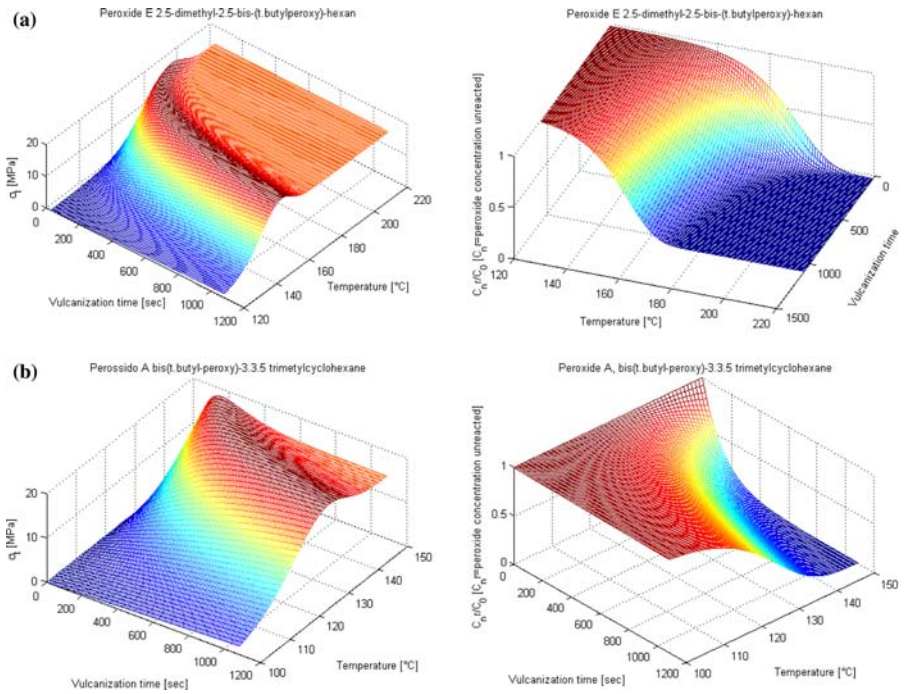

Fig. 8 **a** Peroxide E, tensile strength at different rubber temperatures and exposition times. **b** Peroxide E, unreacted peroxide concentration at different temperature and exposition times. **a** Peroxide A, tensile strength at different rubber temperatures and exposition times. **b** Peroxide A, unreacted peroxide concentration at different temperature and exposition times

Finally, it is worth mentioning that we have chosen as objective function σ_t only for the sake of simplicity. No conceptual difficulties arise if other macroscopic mechanical properties are studied, being the quality control choice related only to producers necessities, their testing equipment and the characteristics of the production line.

Furthermore, the numerical procedure presented can be adapted to any parameter chosen as optimization variable and to any peroxide, simply substituting (1) input numerical interpolation functions depicted in Fig. 7 and (2) $t_{1/2} - T$ curves.

4 Kernel of the numerical model adopted

In this section, the basic features of the numerical approach utilized for the optimization of complex 2D/3D rubber thick elements is outlined. The pseudo-code of the algorithm used for the optimization process is summarized in Fig. 9.

Essentially, the following blocks are repeated in the code at different T_c and exposition times:

1. Determination of temperature profiles for each point of the item (i.e. node in the FEM mesh, as will be outlined in the following section). At this aim, heat transmission Fourier's law in 2D/3D dimensions [2,26] is utilized. Since in the most general case, Fourier's equation is partial and differential, a finite element (FEM) strategy is implemented to solve the problem.
2. Determination, for each point of the object, of its final mechanical properties at different temperatures and different exposition times. An optimal vulcanization time at different insulator fixed temperatures exists, where objective function (tensile stress, elongation, tear strength, etc.) is maximized. Since we are interested to evaluate the overall properties of the vulcanized rubber, an averaged objective function is adopted (i.e. the mean tensile strength is maximized).
3. Determination, by means of a non-standard GA procedure of optimal (T_{ci} t_i) input pairs at which output mechanical properties are maximized. GA is used instead of a more traditional subdivision of the bi-dimensional domain (T_c t) into a regular grid because of the prohibitive processing time required by the grid method. It is worth noting, in fact, that a computationally expensive FEM analysis has to be performed at a fixed (T_c t) pair of input parameters.

4.1 Governing partial differential equations

The vulcanization process can be schematically subdivided into two separate phases: in the first, elastomers are exposed to high temperatures in order to activate peroxidic cross-linking and thus vulcanization, followed by a second cooling phase (usually with air or water) in which rubber is kept to ambient temperature.

Let us consider a generic rubber three dimensional object, in which the coefficient of thermal conductivity λ_p, specific heat c_p^p and density ρ_p are regarded as constant. Temperature profiles for each point of the element are obtained solving numerically a partial differential equations system problem. At this aim, Fourier's heat equation law is used [26]. In particular, the heat balance field equation is the following:

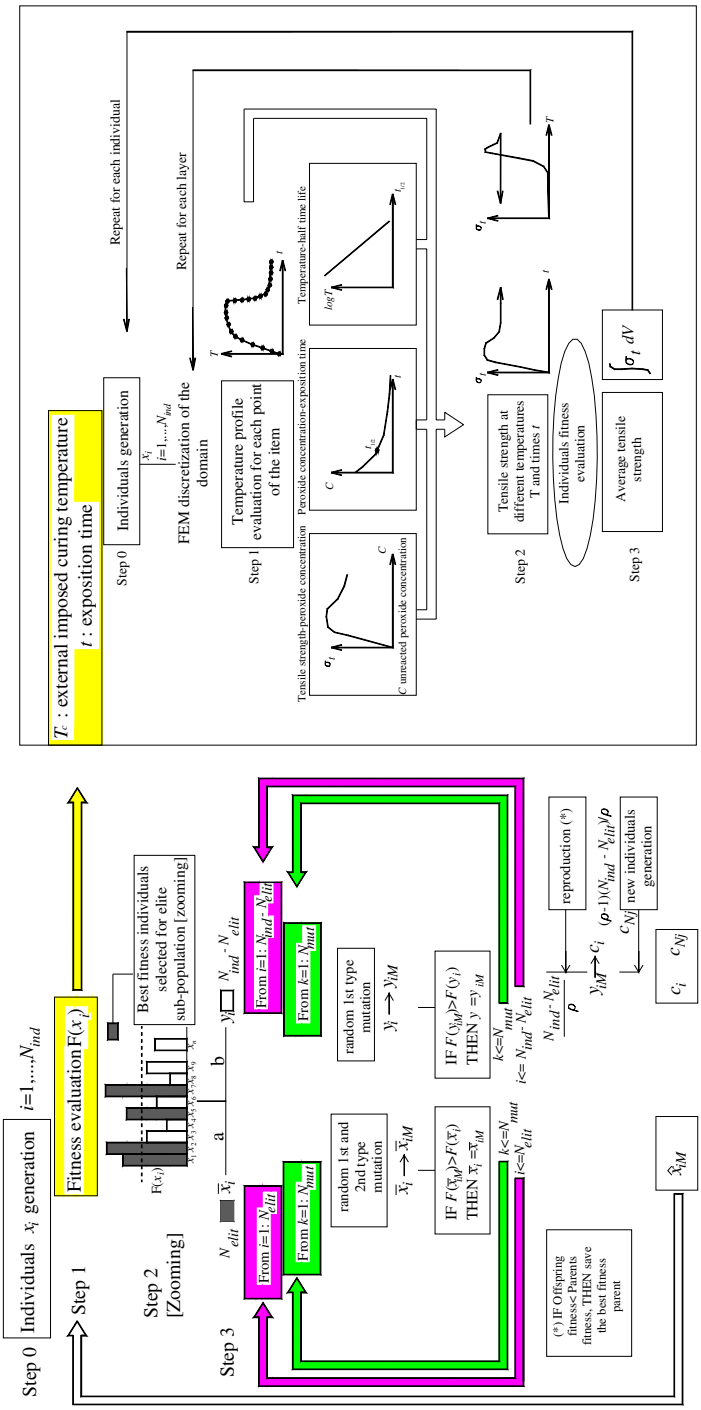

Fig. 9 Schematic representation of the optimization process phases

$$\rho_p c_p^p \left(\frac{\partial T}{\partial t}\right) - \lambda_p \nabla^2 T - r_p \Delta H_r = 0 \tag{7}$$

where:

- ρ_p , c_P^p and λ_p are EPDM density, specific heat capacity and heat conductivity, respectively;
- ΔH_r is rubber specific heat (enthalpy) of reaction and is expressed in kJ/mol;
- r_p is the rate of cross-linking and is expressed in mol/(m^3 s).

It is worth noting that the term $r_p \Delta H_r$ in Eq. 7 is the heat required by the decomposition of the peroxide. ΔH_r, usually ranges from 120 to 180 kJ/mol, representing the bone breaking between oxygen-oxygen in the peroxide. As a rule, $r_p \Delta H_r$ depends on both T and t and several models can be used for an analytical definition of r_p function. Nonetheless, for the sake of simplicity we assume here a constant behaviour for r_p with respect to concentration time first derivative, i.e. $r_p \propto \frac{dC}{dt}$. More complex relations can be adopted [2] in the model proposed without any numerical difficulty. In any case, the contribution of such term in the heat exchange Eq. 7 is small and depends on peroxide concentration in the mixture, which usually is around 1–2% with respect to the blend used.

4.2 Initial and boundary conditions

Two different boundary conditions are applied when dealing with radiation + convection or conduction.

If heat transmission at the external boundary is due to convection + radiation (extrusion process) the following boundary conditions must be applied:

$$\lambda_p \frac{\partial T(\mathbf{P}, t)}{\partial \mathbf{n}(\mathbf{P})} + h(T(\mathbf{P}, t) - T_c) + q_{rad} = 0 \tag{8}$$

where:

- h is the heat transfer coefficient between EPDM and vulcanizing agent at fixed temperature T_c;
- T_c is vulcanizing agent (e.g. nitrogen) temperature;
- $\mathbf{P}$ is a point on the object surface and $\mathbf{n}$ is the outward versor on $\mathbf{P}$;
- q_{rad} is the heat flux transferred by radiation. Radiation contribution for the vulcanization of complex 3D geometries may not be determined precisely. At a first glance, the simplified following formula may be applied:

$$q_{rad} = \sigma \left(T_c^4 - T(R_p, t)^4\right) \Big/ \left[1/\varepsilon_p + \frac{A_p}{A_c}(1/\varepsilon_c - 1)\right] \tag{9}$$

where:

- $\sigma = 5.67 \cdot 10^{-8} \frac{\mathrm{W}}{\mathrm{m^2 K^4}}$ is the Stefan–Boltzmann constant;

– $\varepsilon_{p,c}$ are emissivity coefficients;
– $A_{p,c}$ are the areas of heat exchange (p: insulator, c: curing agent).

When dealing with a compression molding process, the external boundary of the 3D element is subjected to the constant temperature T_c of the steel matrix at increasing time, i.e.:

$$T(\mathbf{P}) = T_c \quad \forall \mathbf{P} \in \partial\Omega \tag{10}$$

where $\mathbf{P}$ is a point on the boundary surface $\partial\Omega$.

When dealing with the cooling phase, no differences occur with respect to the curing process, provided that the temperature of the cooling agent is known at increasing time steps.

Both for extrusion and molding, heat exchange during the cooling phase occurs for convection, i.e. following the partial differential equation:

$$\lambda_p \frac{\partial T(\mathbf{P}, t)}{\partial \mathbf{n}(\mathbf{P})} + h_w(T(\mathbf{P}, t) - T_w) = 0 \tag{11}$$

where h_w is the water (air) heat transfer coefficient, T_w is the water (air) cooling temperature and all the other symbols have been already introduced.

Initial conditions on temperatures at each point at the beginning of the curing process are identically equal to the ambient temperature (hereafter fixed equal to 25 °C for the sake of simplicity), whereas initial conditions at the beginning of the cooling phase are obtained from the temperature profiles evaluated at the last step of the cooling zone, i.e. at $T(\mathbf{P}, t_c)$, where t_c is the total curing time and $\mathbf{P}$ is a generic point belonging to Ω.

4.3 Finite element (FE) implementation: tetrahedrons (3D case) and quadrilateral four-noded elements (2D case)

Partial differential equations system (7)–(11) for complicated geometries and initial temperatures conditions cannot be solved in closed-form. Therefore, in what follows, a Finite Element (FEM) [22,27,28] discretization of the domain is utilized to obtain a reliable approximation of temperatures at each element point and at successive time steps. The procedure has been completely implemented in Matlab [29] language. In this way, resultant FE temperature profiles at each time step are directly collected from the numerical analysis and utilized for the evaluation of output rubber mechanical properties by means of an integrated tool.

When dealing with 3D rubber objects, tetrahedron four-noded elements have been used, see Fig. 10.

Temperature field interpolation is assumed linear inside each element, i.e.:

$$T(\mathbf{P}) = \mathbf{N}^e \mathbf{T}^e \tag{12}$$

where:

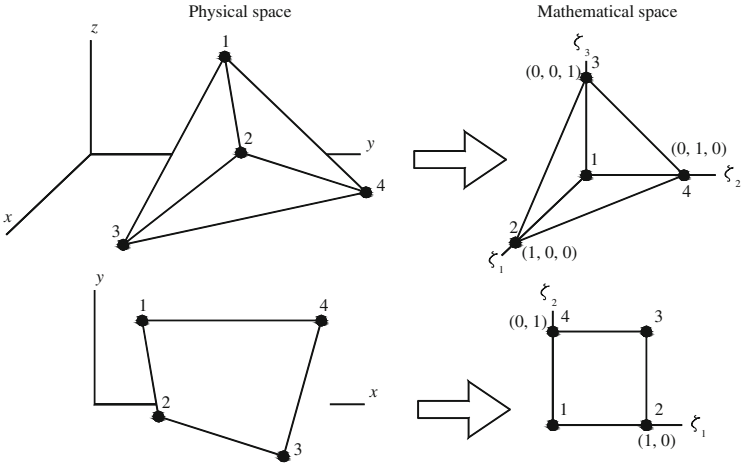

Fig. 10 Four-noded tetrahedrons and four-noded quadrilateral elements used for the 3D and 2D thermal transient analyses (*left*: physical space, *right*: mathematical space)

– $\mathbf{T}^e = [\, T^1 \; T^2 \; T^3 \; T^4 \,]^T$ is the vector of nodal temperatures;
– $\mathbf{N}^e = [\, N^1 \; N^2 \; N^3 \; N^4 \,]$ is the vector of so-called shape functions N^i $(i = 1, \ldots, 4)$;
– $\mathbf{P}$ is a point of coordinates x_P, y_P and z_P.

Indicating with $\mathbf{X}_i = (x_i, y_i, z_i)$ tetrahedron vertices (i.e. nodal) coordinates, N^i are expressed by the following relation:

$$\begin{aligned} \mathbf{X} &= \sum_{i=1}^{4} N_i(\xi_1, \xi_2, \xi_3)\mathbf{X}_i \\ N^i &= \begin{cases} 1 - \xi_1 - \xi_2 - \xi_3 & i = 1 \\ \xi_{i-1} & i = 2, 3, 4 \end{cases} \end{aligned} \tag{13}$$

where $\mathbf{X}$ is a point internal to the tetrahedron (coordinates $(\, x \; y \; z \,)$), $\xi_i \in [\, 0 \; 1 \,]$ is a normalized coordinate and vertices nodes are obtained alternatively imposing $\xi_j = 1$ and $\xi_i = 0$ for $i \neq j$ (except for node $i = 1$ obtained assuming identically $i = 0$).

When dealing with 2D rubber objects, quadrilateral four-noded elements have been used, see Fig. 10.

In this case, temperature field interpolation is quadratic inside each element, i.e.:

$$T(\mathbf{P}) = \mathbf{N}^e\mathbf{T}^e \tag{14}$$

With meaning of the symbols analogous to that of Eq. 12.

In this case, shape functions are expressed by the following equation:

$$N^i(\xi_1, \xi_2) = \frac{1}{4}\left(1 + \xi_1^i\xi_1\right)\left(1 + \xi_2^i\xi_2\right) \quad i = 1, 2, 3, 4 \tag{15}$$

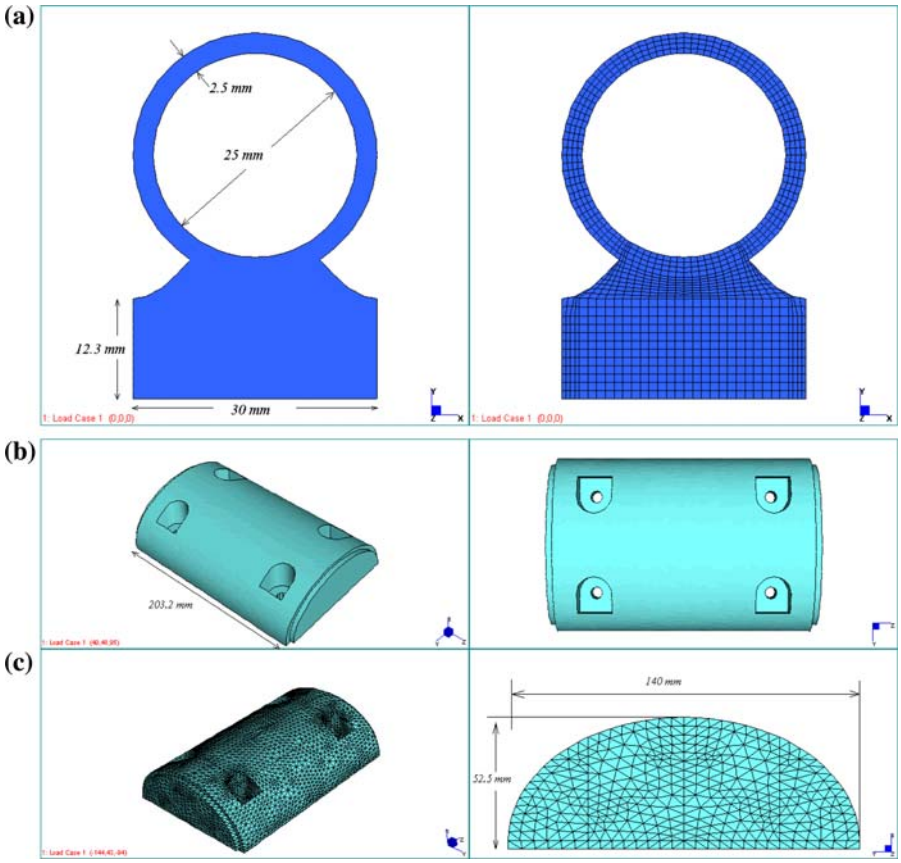

Fig. 11 Geometry and FEM discretization by means of **a** four noded quadrilateral elements and **b** four-noded tetrahedrons of the 2D and 3D items analyzed

where ξ_1^i and ξ_2^i are the so called "natural coordinates" of node i ($\xi_1^i = -1; 1; 1; -1$ and $\xi_2^i = -1; -1; 1; 1$ for $i = 1; 2; 3; 4$, respectively).

In the numerical simulations reported in what follows, the following parameters have been used (see [1]): EPM/EPDM density $\rho_p = 922\,\text{Kg/m}^3$, rubber specific heat capacity $c_p^p = 2,700\,\text{J/(kg °C)}$, $\lambda_p = 0.335\,\text{W/(m °C)}$, $\Delta H_r = 180\,\text{kJ/mol}$, water heat transfer coefficient $h_w = 1490.70\,\text{W/(m}^2\text{°C)}$, curing agent heat transfer coefficient $h = 900\,\text{W/(m}^2\text{°C)}$ [only in case of convection and radiation], $\varepsilon_p = 0.60$, $\varepsilon_c = 0.70$, water cooling temperature $T_w = 25\,\text{°C}$.

Activation energy E_a and $k_{\max}$ depend on the peroxide used, Eq. 3. As a rule, h_w and h should be derived from well known empirical formulas related to laminar/turbulent flow of fluids, see [2] for details, nevertheless here characteristic values are used for the sake of simplicity.

Geometries of the 3D (docks bumper) and 2D (weather strip) rubber elements analyzed in this paper are shown in Fig. 11. In Figs. 12 and 13, two temperature color patches at increasing instants referred to the 2D and 3D items, respectively are

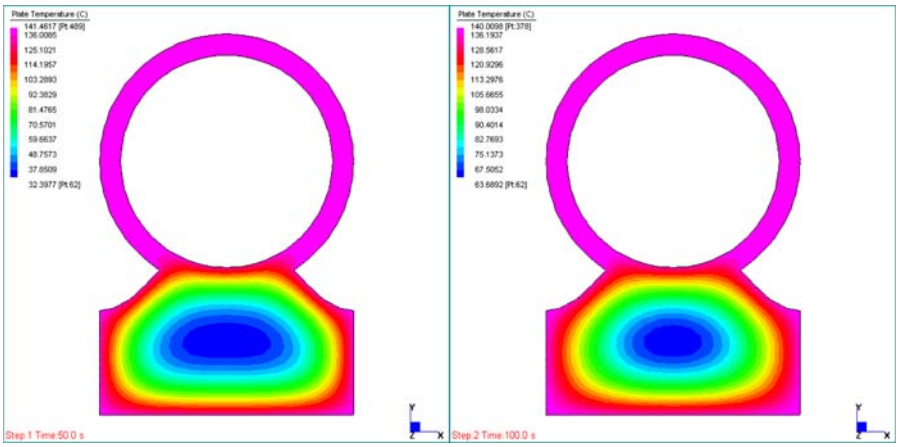

Fig. 12 2D weather strip. Temperatures distribution resulting from the FEM analysis at two different time steps with $T_c = 140\,^{\circ}\mathrm{C}$. (Color figure online)

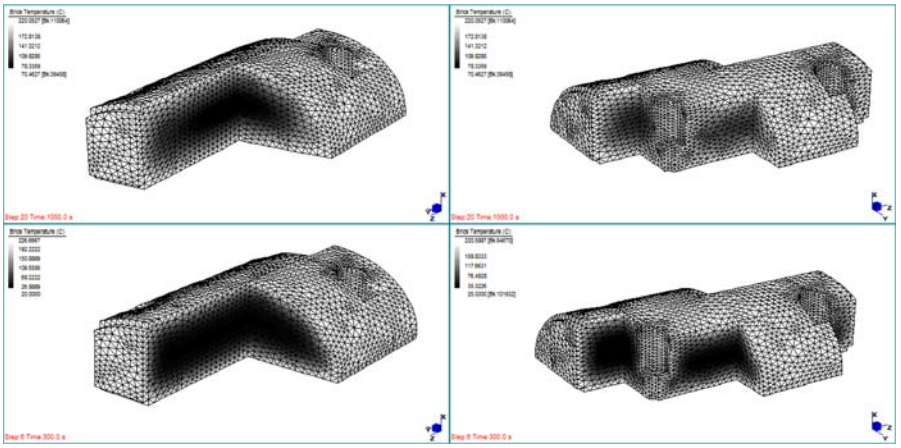

Fig. 13 3D docks bumper. Temperatures distribution resulting from the FEM analysis at two different time steps with $T_c = 220\,^{\circ}\mathrm{C}$. (Color figure online)

reported. As it is possible to notice, internal points remain at a relatively cool temperature, especially for the 3D case (Fig. 13) even at the end of the vulcanization process.

In order to have a deep insight into this phenomenon (typical of thick items), in Fig. 14, temperature patch for the 3D docks bumper (only 1/4 of the mesh is shown) are reported at 6,000 and 2,500 s, assuming $T_c = 160\,^{\circ}\mathrm{C}$ and highlighting two different nodes with colored dots (one is a node near the external surface, whereas the other belongs to the internal core). In the simulations, a 50–50% of Peroxide A and E is used.

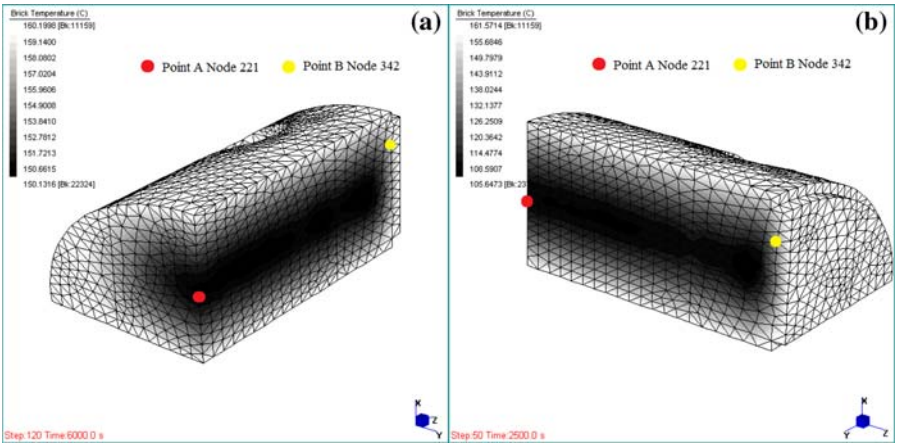

Fig. 14 Temperature profile of 3D item at $T_c = 160\,^{\circ}\mathrm{C}$ and position of nodes inspected (1/4 of the item is shown). **a** 6,000 s. **b** 2,500 s. (Color figure online)

Temperature-time, residual peroxides concentration vs time and tensile strength diagrams for the two nodes are reported in Figs. 15 and 16, respectively, assuming a curing time equal to 4,400 s.

As it is possible to notice, Point A reaches a good level of vulcanization (Fig. 15c), which is also addressed by the residual unreacted concentration of one of the two peroxides (Fig. 15b). On the contrary, Point B results over-vulcanized (Fig. 16c), meaning that both peroxides residual concentration is negligible (Fig. 16b). As one cannot, it is particularly evident the difference in the resulting tensile strength at the end of the vulcanization process, a direct consequence of the different temperature profiles of the two nodes (compare Figs. 15a and 16a). Form the simulations, it is worth noting the existance of an optimal $t - T$ point at which σ_t reaches its maximum for the node of the mesh under consideration, which corresponds to a specific value of unreacted peroxide concentration in the mixture.

5 The genetic algorithm proposed

The evaluation of optimal ($T_c t$) input pairs for the problem at hand can be easily tackled with genetic schemes [30–34], avoiding in this way procedures based on non-linear optimization approaches. In particular, the advantage is represented by (a) the theoretical simplicity of the procedure itself, (b) the robustness and efficiency in terms of time required for the optimization and (c) its application to the case in which objective function is not known analytically. For the problem at hand, point (c) is crucial, leading to prefer stochastic and/or meta-heuristic approaches instead of classic methods. In fact, in this case, temperature profiles (which give by integration the objective function) are derived from a finite elements numerical solution of a PDEs system, thus leading to a non linear optimization problem in which objective function is not analytically known.

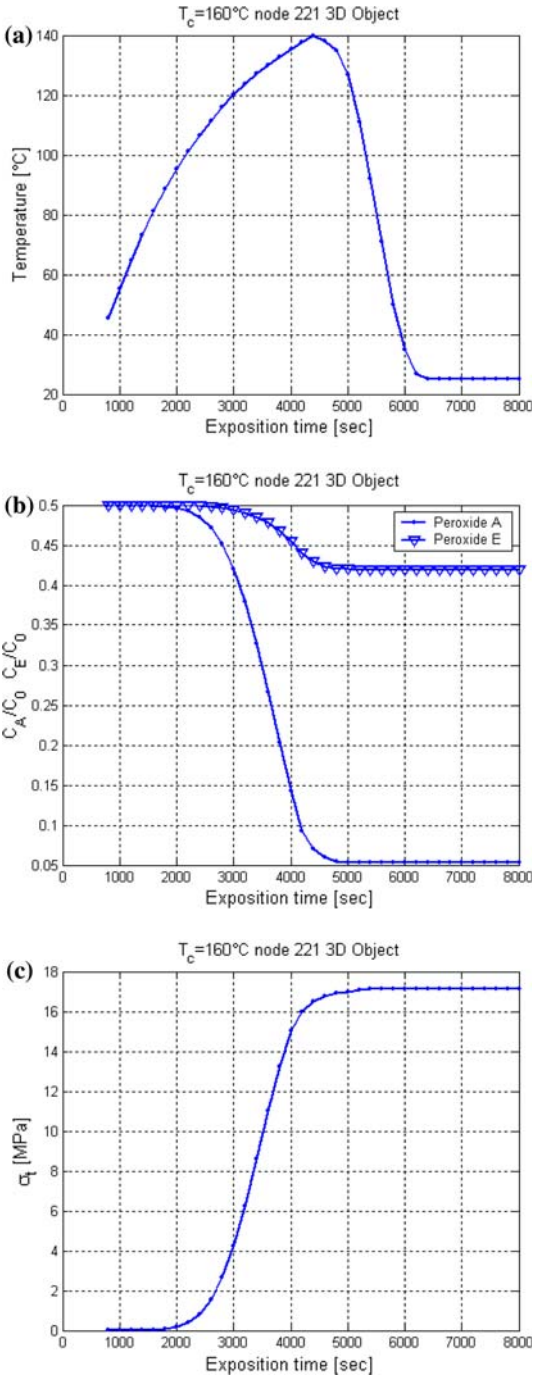

Fig. 15 Point A (Node 221) **a** $t - T$, **b** t-peroxide concentration and **c** $t - \sigma_t$ curves. In the case analyzed $\chi = 0.5$

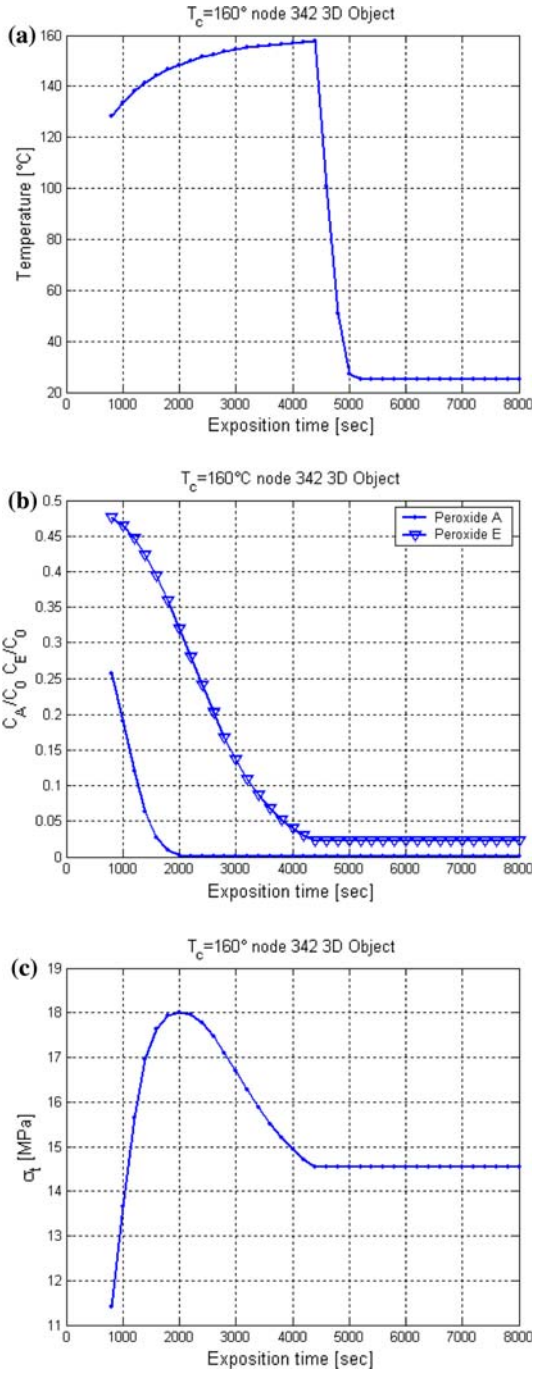

Fig. 16 Point B (Node 342) **a** $t - T$, **b** t-peroxide concentration and **c** $t - \sigma_t$ curves. In the case analyzed $\chi = 0.5$

In general, a genetic algorithm (GA) is a stochastic global search method that mimics the metaphor of natural biological evolution. At a first attempt, see Goldberg [30], the GA algorithm here proposed classically operates on a population of potential solutions applying the principle of survival of the fittest to produce better and better approximations to a solution. At each generation, a new set of approximations is created by the process of selecting individuals according to their level of fitness in the problem domain and breeding them together using operators borrowed from natural genetics. This process leads to the evolution of populations of individuals that are better suited to their environment than the individuals that they were created from.

In particular, the kernel of the GA proposed is a set of standard genetic operations consisting of reproduction, crossover and mutation and non standard procedures, such as zooming and elitist strategy [35,36]. Each individual is represented by an admissible temperature and exposition time, i.e. a sequence of individuals i in the form $\left(T_c^i \; t^i\right)$. Since individuals are stored as a sequence of two real positive numbers, their encoding by means of binary strings results particularly easy. In this way, the genotypes (chromosome values) can be uniquely mapped onto the decision variable (phenotypic) domain. In a standard GA procedure, the use of Gray coding is necessary to avoid a hidden representational bias in conventional binary representation as the Hamming distance between adjacent values is constant (see [31,32]).

For standard operators (mutation, crossover, reproduction), a concise description of both the mathematical background and the parameters adopted is reported in what follows (the reader is referred to [30,32] for details).

The algorithm can be summarized as follows:

1. Step 0: An admissible initial population $\mathbf{x} = \{x_i : i = 1, \ldots, N_{ind} | x_i \text{ admissible}\}$ is randomly generated at the first iteration;
2. Step 1: x_i fitness $F(x_i)$ is evaluated solving numerically a PDEs system with fixed x_i;
3. Step 2: Two sub groups are created, denoted as $\overline{\mathbf{x}} = \{\overline{x}_i : i = 1, \ldots, N_{elit} | x_i$ admissible$\}$ and $\mathbf{y} = \mathbf{x} - \overline{\mathbf{x}} = \{y_i : i = 1 :, \ldots, N_{ind} - N_{elit}\}$, respectively. $\overline{\mathbf{x}}$ is the group of all the individuals with the N_{elit} (user defined) higher fitness values (zooming strategy).
4. Step 3a: For each $\overline{x}_i$, a random improvement of the individual (in terms of fitness) is tried, by means of two different mutation operators (1st and 2nd type, as described in what follows). The recursive double operation (applied randomly N_{mut} and N_{mut2} times) leads to new individuals generation $(\overline{x}_{iM})$, which overwrite the original $\overline{x}_i$ only if their fitness $F(\overline{x}_{iM})$ is greater than $F(\overline{x}_i)$. At the end of the double loop, a new sub-group $\overline{\mathbf{x}}_M = \{\overline{x}_{iM} : i = 1, \ldots, N_{elit} | \overline{x}_{iM}$ admissible$\}$ is obtained.
5. Step 3b: For each y_i, a mutation loop (only 1st type mutation) is applied randomly N_{mut} times, leading to an improvement of y_i fitness. The new individuals y_{iM} overwrite the original y_i only if their fitness is greater than y_i one (elitist approach). At the end of the double loop, a new sub-group $\mathbf{y}_M = \{y_{iM} : i = 1, \ldots, N_{ind} - N_{elit} | y_{iM}$ admissible$\}$ is obtained. A classic reproduction operator is applied only for individuals of $\mathbf{y}_M$ with high fitness (i.e. on $(N_{ind} - N_{elit})/\rho$ parents with user defined parameter $\rho > 1$) in order to create a new offspring group $\mathbf{c}$. The remaining

$(1-\rho)(N_{ind}-N_{elit})/\rho$ individuals are generated *ex-novo* using Step 0 procedure and are catalogued into $\mathbf{c}_N = \{c_{Nj} : j : 1, \ldots, (N_{ind}-N_{elit})/\rho | c_{Nj}$ admissible$\}$.

6. Step 4: The final population at the i-th iteration is collected into $\mathbf{x} = [\,\overline{\mathbf{x}}_M\ \mathbf{c}\ \mathbf{c}_N\,]$ and the procedure is repeated *ad libitum* from Step 1.

The implementation of non-standard strategies (zooming with elitist strategy) is necessary in order to obtain a considerable enhancement of both robustness and efficiency of the algorithm. In particular, authors experienced that standard generalist GAs at disposal in commercial packages usually show a slow convergence and sometimes fail to reach an optimal admissible solution, even using large populations.

5.1 Generation of admissible individuals

The generation of admissible individuals occurs by means of random processes respecting all admissibility conditions ($T_c > 0$ and $t > 0$). Such a procedure is followed at the first iteration (for all the N_{ind} individuals) and at each iteration $i > 1$, see Fig. 9, for $(\rho-1)(N_{ind}-N_{elit})/\rho$ individuals. A binary representation with chromosomes is used for each individual in the population. If, as is the case here treated, the number of optimization variables (here denoted as N_{var}) is 2 (i.e. a 2D optimization problem in T_c and t has to be solved) each individual is represented by $N_{bit} = N_{bit}^1 + N_{bit}^2$ chromosomes.

Thus, the population has N_{bit} chromosomes and is an $N_{ind} \times N_{bit}$ matrix filled with random ones and zeros generated using the following syntax [32]:

$$\text{pop} = \text{round}(\text{rand}(N_{ind}, N_{bit})) \tag{16}$$

where the function rand$(N_{ind}, N_{bit}\ )$ generates a $N_{ind} \times N_{bit}$ matrix of uniform random numbers between zero and one. The function round rounds the numbers to the closest integer which in this case is either 0 or 1. Each row in the pop matrix is obviously an individual encoded with chromosomes. The chromosomes correspond to discrete values of T_c and t. In order to pass from a binary representation to a continuous representation, a so called quantization error is introduced. Obviously, increasing the number of bits reduces the quantization error. Furthermore, an upper bound limitation is introduced for T_c and t variables, assuming for all the examples treated that $T_c < T_c^{\max} = 400\,^{\circ}\text{C}$ and $t < t^{\max} = 25,200$ s = 7 h. In fact, unbounded variables should require, at least from a theoretical point of view, an infinite number of bits for their encoded representation. In what follows, in order to introduce a negligible quantization error, a 8 + 8 bits representation is used for individuals. Next, the variables are passed to the cost function for evaluation.

5.2 Reproduction

The reproduction phase is applied to $\mathbf{y} = \{y_i : i = 1 : N_{ind} - N_{elit}\}$ group. As usual, for each individual, a fitness value derived from its raw performance measure given by the objective function is assigned. This value is used in the selection to bias towards

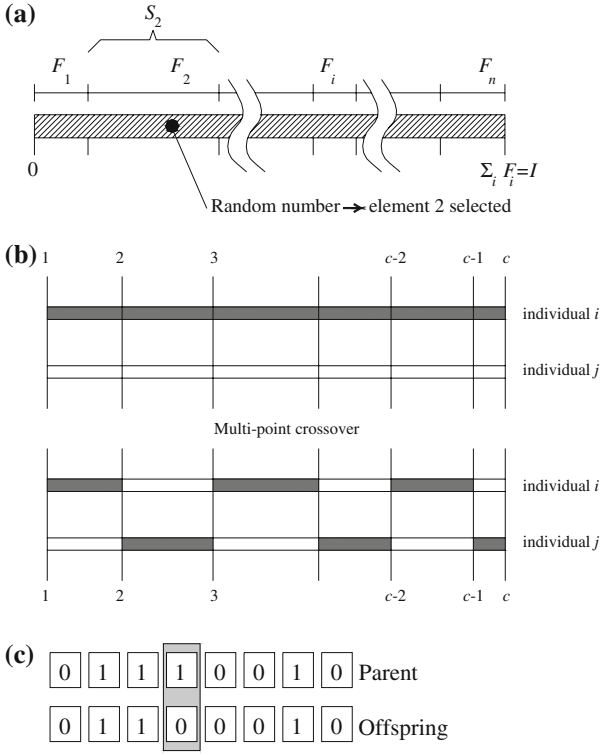

Fig. 17 Selection operation-roulette wheel-(**a**), crossover (**b**), mutation (**c**)

more fit individuals. Highly fit individuals, relatively to the whole population, have a high probability of being selected for mating whereas less fit individuals have a correspondingly low probability of being selected.

Once the individuals have been assigned a fitness value, they can be chosen from the population, with a probability according to their relative fitness, and recombined to produce the next generation.

A stochastic sampling with replacement (roulette wheel) is used here. An interval I is determined as the sum of the fitness values F_i of all the individuals in the current population, i.e. $I = \sum F_i$. For each individual i, a sub-interval S_i corresponding to its fitness value in the interval $[0\ I]$ is determined, i.e $S_i = F_i$, so that $I = \sum S_i$ and the size of the interval associated to each individual is proportional to its fitness, i.e. so that a big sub-interval corresponds to a highly fit individual. To select an individual, a random number is generated in the interval $[0\ I]$ and the individual whose segment sub-interval spans the random number is selected, see Fig. 17a. This process is repeated until the desired number of individuals have been selected.

Reproduction is active only on **y** sub-population. Only an offspring per pair is generated and a total number of $(N_{ind} - N_{elit})/\rho$ of reproductions is allowed. The remaining $(\rho - 1)(N_{ind} - N_{elit})/\rho$ individuals are generated ex-novo. This procedure, which mimics the biological behaviour of an open population, assures a stochastic

possibility of introduction of new chromosomes (i.e. individuals) with good characteristics in terms of fitness.

5.3 Zooming and elitist strategy

The application of an *ad hoc* technique for the problem at hand is required in order to obtain improved and reliable results in terms of best fitness at each iteration. As already pointed out, the kernel of the algorithm relies in sub-dividing the initial population into two groups:

$$\begin{aligned} \overline{\mathbf{x}} &= \{\overline{x}_i : i = 1, \ldots, N_{elit} | x_i \text{ admissible}\} \\ \mathbf{y} &= \mathbf{x} - \overline{\mathbf{x}} = \{y_i : i = 1, \ldots, N_{ind} - N_{elit}\} \end{aligned} \tag{17}$$

The so called zooming strategy consists in collecting at each iteration the individuals with higher fitness into an "elite" sub-population $\overline{\mathbf{x}}$ (with user defined dimension N_{elit}). Then, for each individual belonging to group $\overline{\mathbf{x}}$, only mutation (with high probability) is applied in order to improve individuals fitness. Two different mutation algorithms are utilized, differing only on the number of cells of each individual involved by the mutation process.

Subsequently, an elitist strategy preserves the original individual if mutation results in a reduction of individual fitness, whereas zooming technique restricts search domain, so improving in any case convergence rate. Unfortunately, no theorems are available for assuring an unconditioned convergence of the method in any case, as well as no theoretical rules can be given in the choice of both reproduction and mutation schemes. Even if this limitation could appear rather important, it is always implicitly accepted that meta-heuristic approaches do not assure convergence at the desired solution without limitations. Only experience in the numerical simulations of specific problems can help in the correct choice of input parameters [35,36].

From a practical point of view, zooming is set by means of the so called zooming percentage $z_{\%}$, defined as the percentage ratio between $\mathbf{x}$ initial population and $\overline{\mathbf{x}}$ sub-population dimension, i.e.:

$$z_{\%} = \frac{N_{elit}}{N_{ind}} 100 \tag{18}$$

5.4 Crossover

During a generation of a new individual from two parents, a crossover operator is used to exchange genetic information between pairs.

In the present study, we use a multi-point crossover operator, which works as follows: $k_i = [\,1\ 2\ \ldots\ c-1\,]$ crossover points are randomly selected on two individuals (parents) represented by c chromosomes (bits), as shown in Fig. 17b. Bits between the crossover points are exchanged between the parents in order to produce a new offspring.

5.5 Mutation

Mutation is generally considered to be a background operator that ensures that the probability of searching a particular subspace of the problem space is never zero. In the present algorithm, mutation is applied with high probability directly on existing individuals and two different algorithms (here denoted as 1st and 2nd type) are applied. Mutation is a fundamental task that permits a strong fitness improvement at each iteration.

- *First type mutation*

Such operator is the classic mutation and is applied both on $\overline{\mathbf{x}}$ and $\mathbf{y}$ individuals. For each individual $\overline{\mathbf{x}}_i$ (or $\mathbf{y}_i$) it works stochastically on all the chromosomes (i.e. changing at random one of the individual columns from 1 to N_{bit}), Fig. 17c. The procedure is repeated once on N_{mut} different individuals. Obviously, first type mutation results in a new individual in which only one of the optimization variables T_c and t, after chromosomes decoding, results changed with respect to the original individual.

- *Second type mutation*

Second type mutation is applied only to $\overline{\mathbf{x}}$ individuals, in order to obtain a further improvement of their fitness. It works analogously to the first type algorithm, with the only difference that it changes, for the individual subjected to mutation, a chromosome belonging to T_c and one belonging to t. Thus, the resulting individual after chromosomes decoding is different from the original both in T_c and t. The procedure is repeated on N_{mut2} individuals.

Both N_{mut} first type mutations and N_{mut2} second type mutations are user defined.

The final result of the application of both first and second type mutation is a new admissible individual (Fig. 9) $\overline{x}_{iM}$ with different fitness with respect to $\overline{x}_i$. If $\overline{x}_{iM}$ fitness is higher than that of the original individual (note that the check is executed at each N_{mut} iteration), $\overline{x}_i$ is overwritten with $\overline{x}_{iM}$.

6 Numerical simulations

Two sets of numerical simulations are reported in this section, in order to show the improvement of output rubber mechanical properties when mixtures of two peroxides with different molar ratios are considered. In the first example, the two dimensional (relatively thin) weather strip rubber item obtained by extrusion is considered (Fig. 11a), whereas in the second example the 3D object of Fig. 11b is analyzed.

It is worth mentioning here that the 2D item is obtained by hot extrusion, i.e. the polymer is heated to molten state by a combination of heating elements and shear heating from the extrusion screw. Immediately after, the screw forces the resin through the die, forming the rubber into the desired shape. Obviously, during vulcanization, the item changes its shape and therefore the procedure aforementioned described is only approximate. Nevertheless, it certainly represents a valuable reference solution to calibrate input parameters and has the same degree of approximation of existing literature at disposal [27,28].

Optimal input parameters functions $\hat{T} = \hat{T}(T_c, t) = 0 | \hat{T} \equiv \{P^i = (T_c^i, t^i) \text{ optimal}\}$ are obtained by means of the GA approach proposed for both cases.

In particular, optimal $\hat{T}$ curves (expressed as implicit functions in T_c and t) are numerically evaluated solving point by point the following optimization problem:

$$\begin{aligned} &\max \tfrac{1}{N_L} \sum_{k=1}^{N_L} \sigma_t^k \left(T_c^i, t^i\right) \\ &\text{subject to} \begin{cases} 0 < T_c^i < T_c^{\max} \\ 0 < t^i < t^{\max} \end{cases} \\ &\text{PDEs system} \begin{cases} \rho_p c_p^p \left(\frac{\partial T}{\partial t}\right) - \lambda_p \nabla^2 T - r_p \Delta H_r = 0 \\ \text{boundary and initial conditions} \end{cases} \end{aligned} \tag{19}$$

where N_L is the number of nodes in which the item is discretized and $T_c^{\max}(t^{\max})$ is an upper bound limitation for curing temperature (exposition time).

Results provided by the GA approach proposed are compared with those obtained subdividing $T_c - t$ plane with a regular grid. In the latter case, for each point $P^{i,j} \equiv (T_c^i, t^j)$ of the grid a mixed algebraic-PDEs system has to be solved:

$$\begin{aligned} &\sigma_t = \tfrac{1}{N_L} \sum_{k=1}^{N_L} \sigma_t^k \left(T_c^i, t^j\right) \\ &\text{PDEs system} \begin{cases} \rho_p c_p^p \left(\frac{\partial T}{\partial t}\right) - \lambda_p \nabla^2 T - r_p \Delta H_r = 0 \\ \text{boundary and initial conditions} \end{cases} \end{aligned} \tag{20}$$

Obviously a very large computational effort is required in solving problem (20) using the grid method (otherwise a global optimization algorithm where objective function is not analytically known has to be performed).

For all the numerical simulations reported in this section, the following GA parameters have been used: number of individuals $N_{ind} = 30$, zooming $z_{\%}$ 30%, total number of first and second type mutations $N_{mut} = 8$, parameter ρ equal to 0.5, maximum number of generations $N_{gen} = 40$–60.

In all the simulations, we have chosen different % mixtures of Trigonox 101 (peroxide E) and Trigonox 29 (peroxide A). They have $t_{1/2}$ equal to 6 min, respectively at 171 and 138 °C. Both peroxides are well suited to vulcanize EPM/EPDM rubber, but they are highly active at very different temperatures. Therefore, they seem particularly appropriate to vulcanize thick elements, which need peroxides active in a wide range due to the differences in the temperature profiles between core and skin. At a first attempt and for the sake of simplicity, we suppose that there is no interaction between the two peroxides used (see Eq. 6).

In Fig. 18, tensile strength at 5 different external curing temperatures as a function of exposition time are shown for three different mixtures of peroxides A and E (a: peroxide A only, b: 75% A and 25% E, c: 50% A and 50% E).

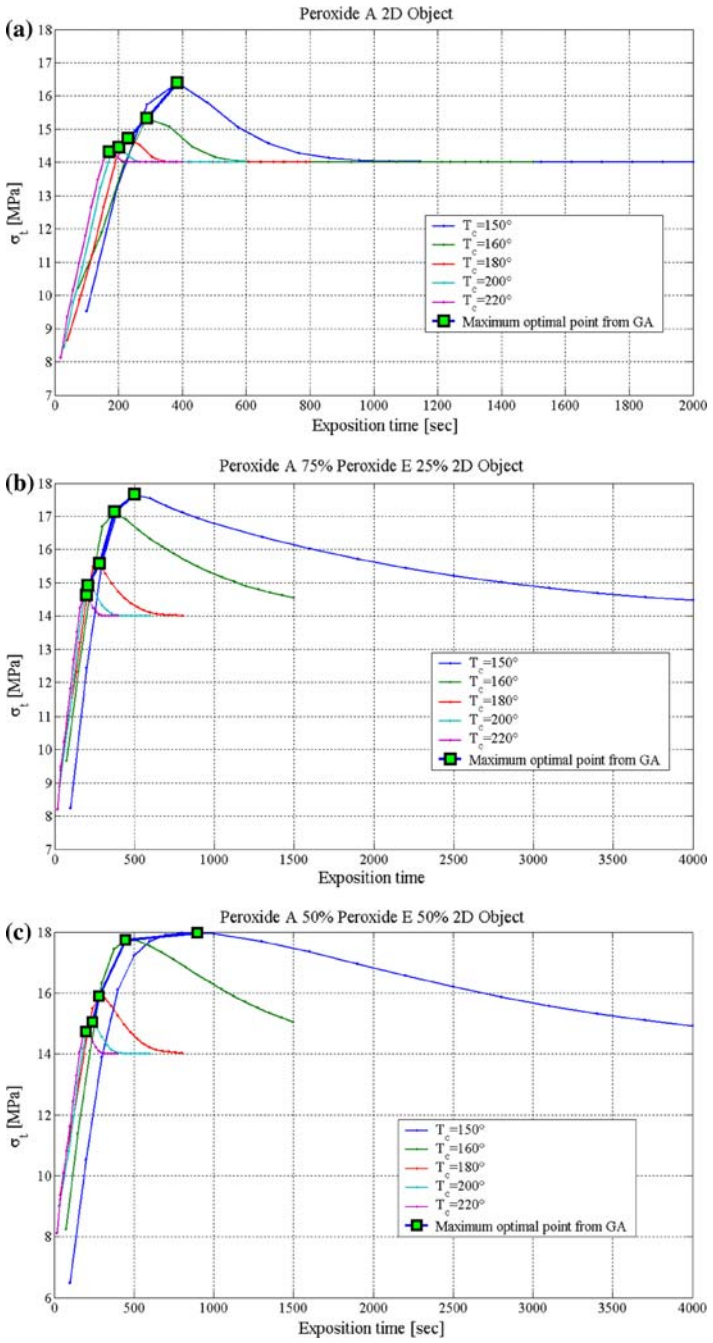

Fig. 18 Resultant tensile strength at different curing times for 5 increasing curing temperatures, 2D object. **a** Peroxide A only. **b** 75% Peroxide A 25% Peroxide E. **c** 50% Peroxide A 50% Peroxide E. *Squares* refer to GA optimized resultant tensile strengths

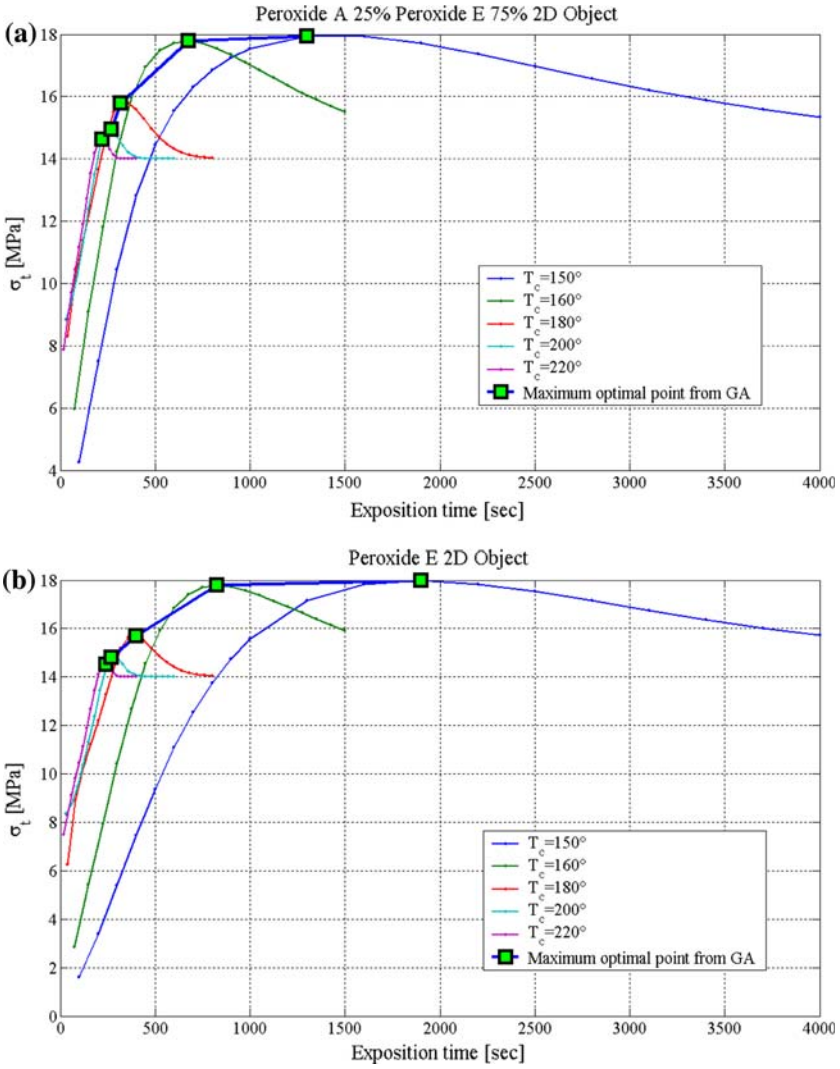

Fig. 19 Resultant tensile strength at different curing times for 5 increasing curing temperatures, 2D object. **a** 25% Peroxide A 75% Peroxide E. **b** Peroxide E only. *Squares* refer to GA optimized resultant tensile strengths

The same simulations results are reported in Fig. 19 for mixtures corresponding to 25% of peroxide A—75% of peroxide E (a) and 100% peroxide E (b).

3D representations of results depicted in Figs. 18 and 19 are also reported in Figs. 20 and 21, respectively for the sake of completeness.

Squares in the diagrams represent GA optimized results. As it is possible to notice from all the figures, optimal output tensile strength value is reached with the simple heuristic approach proposed for each case analyzed, meaning that the procedure

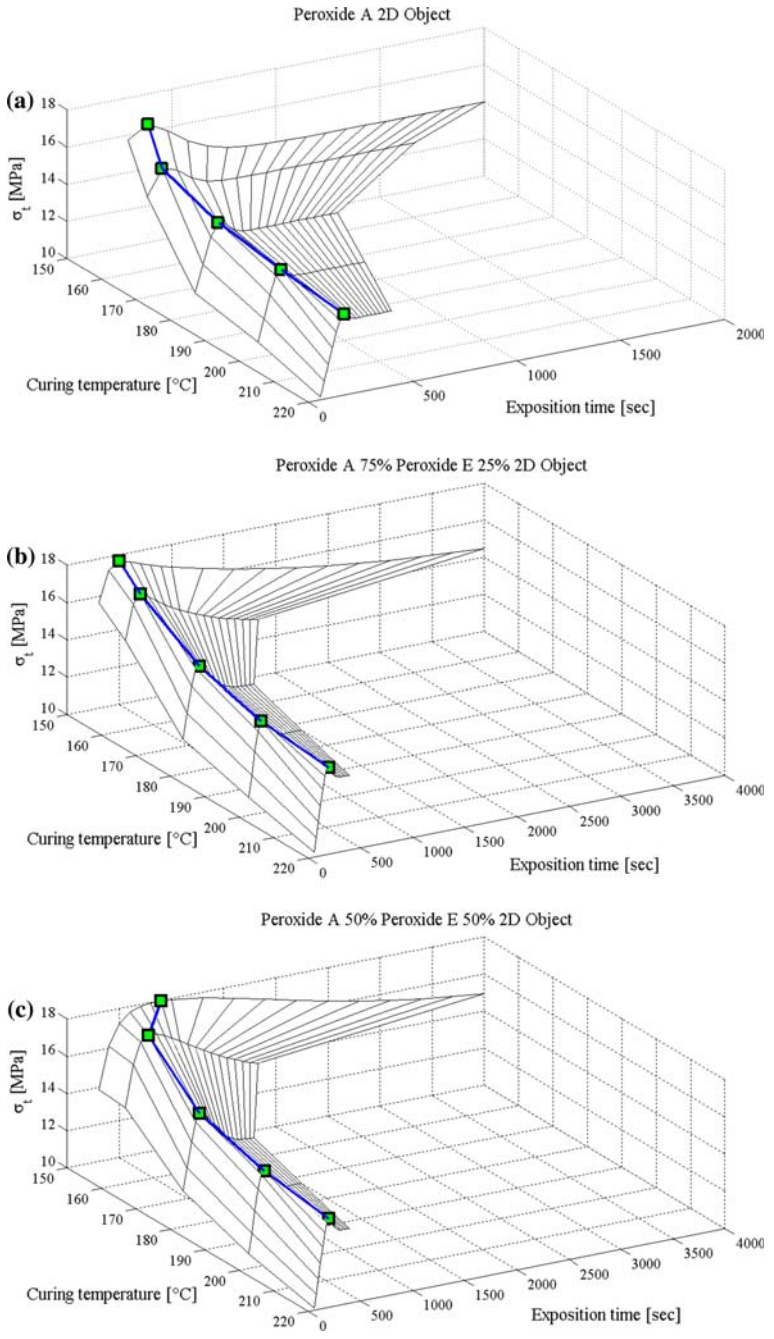

Fig. 20 Resultant tensile strength at different curing times, 2D object, 3D representation. **a** Peroxide A only. **b** 75% Peroxide A 25% Peroxide E. **c** 50% Peroxide A 50% Peroxide E. *Squares* refer to GA optimized resultant tensile strengths

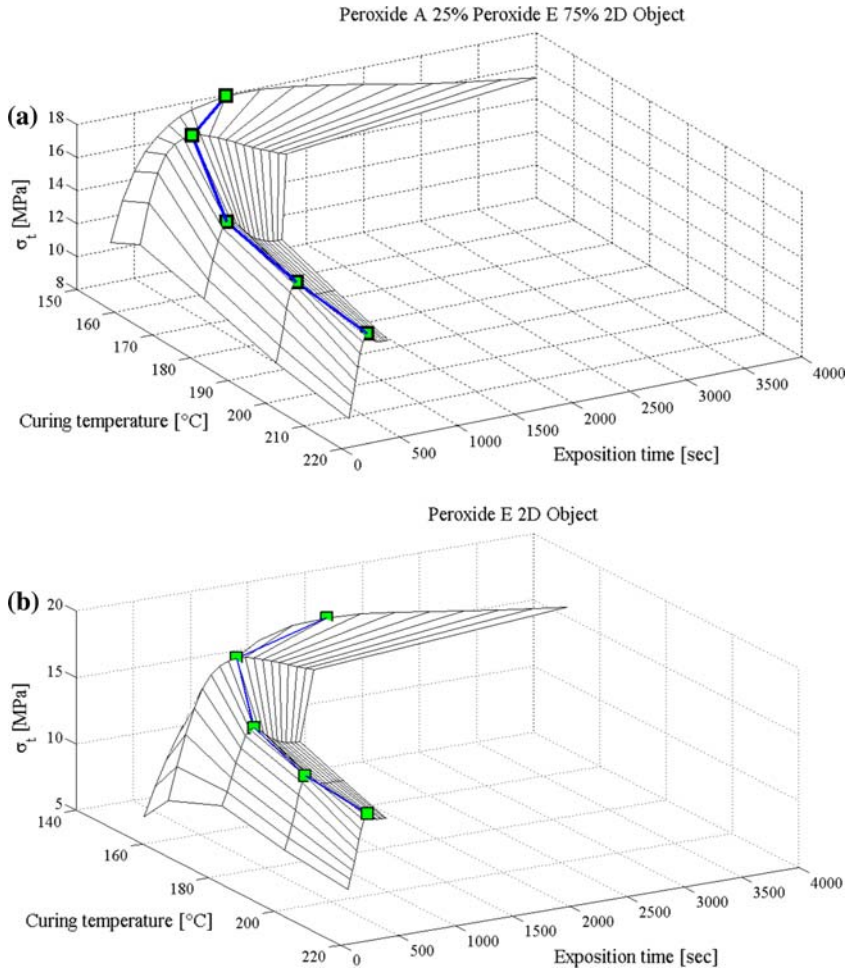

Fig. 21 Resultant tensile strength at different curing times, 2D object, 3D representation. **a** 25% Peroxide A 75% Peroxide E. **b** Peroxide E only. *Squares* refer to GA optimized resultant tensile strengths

proposed may be of interested for practitioners involved in the production process of rubber items.

From the simulations, it can be deduced that the best results are achieved with a mixture of peroxides at 50–50% molar ratio, for all the external curing agent temperatures inspected. As can be noticed from the simulations, the range of optimal temperatures is approximately between 150 and 160 °C. Exceeded 160°, it is yet possible to find optimal values of exposition time, but with a resultant optimized tensile strength which is not sensibly improved with respect to the asymptotic value (i.e. obtained with an over-vulcanization of the item). Such behaviour is due to the fact that, at relatively high temperatures of vulcanization, $t_{1/2}$ values of both peroxides reduce considerably. As a consequence, external layers vulcanization time decreases sensibly, wheareas internal core (which, remaining cooler, does not undergo the same temperature profile

of the external coat) remains essentially under-vulcanized. Therefore, the peak of the optimal average tensile strength results less marked. In any case, simulations show that peroxides mixtures may improve vulcanization quality in terms of (a) optimal value of tensile strength reached and of (b) reduction of time required for the vulcanization. Obviously, manufactures may choose to calibrate (a) typology and (b) molar ratios of the mixtures in agreement with their production constraints in order to improve resultant items quality.

Analogously to the 2D case, in Figs. 22 and 23 final average tensile strengths at successive exposition times for different A and E peroxides mixtures are represented for the 3D docks bumper. In all the cases analyzed, curves are replicated varying external curing agent temperature in a wide range. Finally, in Figs. 24 and 25, the same results are depicted using a 3D representation for the sake of clearness. Analogously to the previous case, a 50–50% molar ratio between the two peroxides guarantee almost the maximum tensile strength at lower time of vulcanization with respect to the utilization of only peroxide E. Optimal vulcanization temperature ranges between 140 and 160 °C. At higher temperatures (especially from 180 to 220 °C), all peroxides mixtures reach the maximum average tensile strength requiring a relatively short exposition time, but maximum value increases insufficiently if compared with the over-vulcanized one. Another important aspect is worth noting, related to the optimal exposition time required for the vulcanization. When dealing with 3D thick objects, in fact, optimal value is around 5–10 times longer with respect to the 2D case. Obviously, this is a consequence of the different thickness of the two items (see Fig. 11), which makes the vulcanization of 3D objects core a very difficult task.

An overall analysis of simulations results underlines that: (a) items dimensions and (b) peroxides half life time are key issues for the determination of vulcanization time and temperature.

Furthermore, it appears clear that the utilization of peroxides mixtures can increase resultant tensile strength (and thus improving final item quality) or can reduce curing time at fixed output mechanical properties. In any case, different mixtures percentages influence optimal $\hat{T}$ loci extensively. Therefore, it appears particularly useful from a practical point of view the numerical determination of $\hat{T}$ functions at different percentage mixtures.

7 Conclusions

A numerical procedure for the determination of optimal input parameters (curing temperature and exposition time) for 2D/3D thick EPM/EPDM items in presence of different mixtures of peroxides has been presented. Vulcanization external temperature T_c, rubber exposition time t and different peroxides mixtures have been assumed as production parameters to optimize.

Objective function is represented by rubber final mean tensile strength after vulcanization. Despite the fact that the analyses presented are limited only to the utilization of two input variables and one output mechanical property, the algorithm proposed can be applied without any conceptual difficulty in a more general framework. Furthermore, the same mathematical approach presented can be extended for other polymeric systems that can be vulcanized by peroxides.

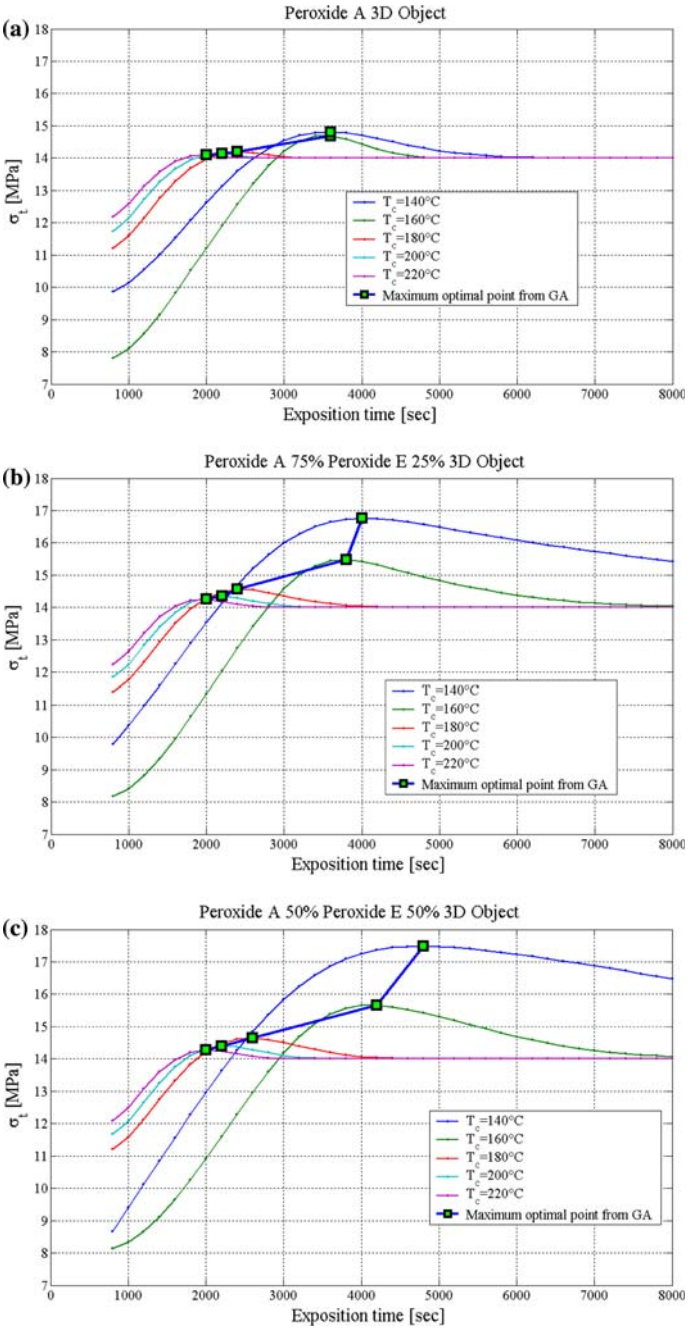

Fig. 22 Resultant tensile strength at different curing times for 5 increasing curing temperatures, 3D object. **a** Peroxide A only. **b** 75% Peroxide A 25% Peroxide E. **c** 50% Peroxide A 50% Peroxide E. *Squares* refer to GA optimized resultant tensile strengths

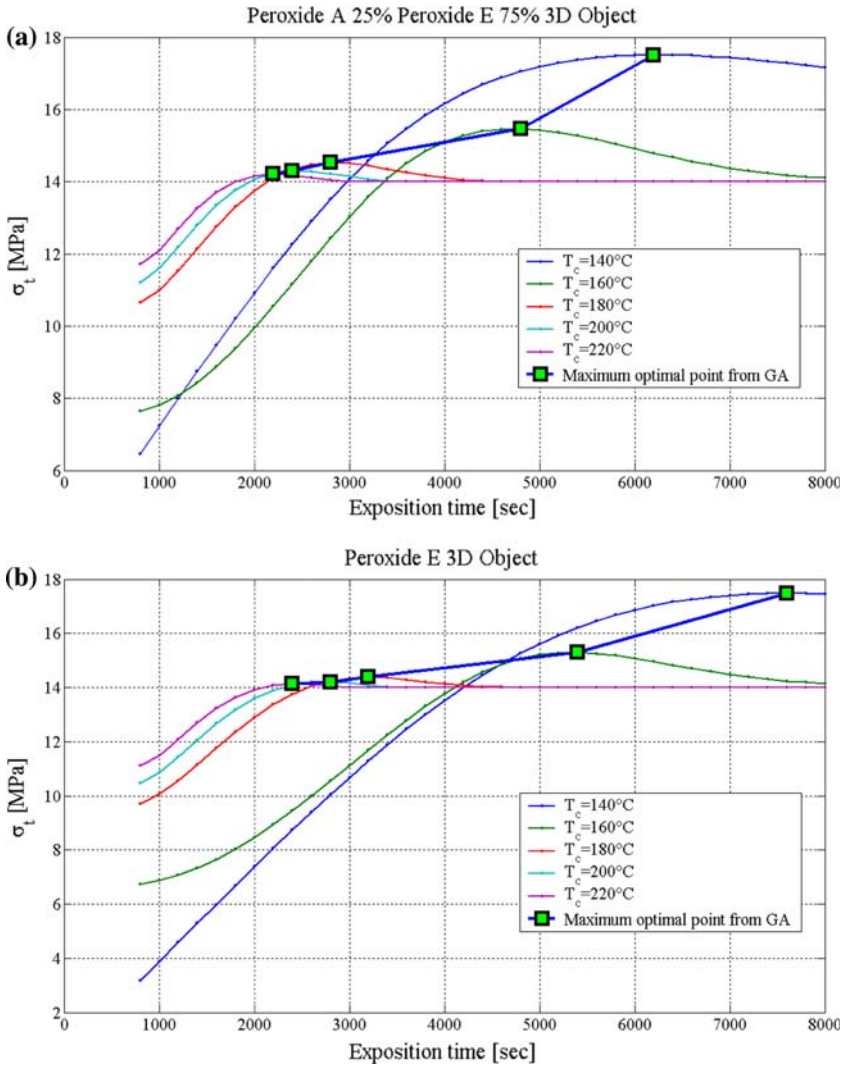

Fig. 23 Resultant tensile strength at different curing times for 5 increasing curing temperatures, 3D object. **a** 25% Peroxide A 75% Peroxide E. **b** Peroxide E only. *Squares* refer to GA optimized resultant tensile strengths

In order to avoid the utilization of a numerically expensive grid of points, a genetic algorithm with zooming and elitist strategy has been used for the determination of optimal production parameters.

Two meaningful examples of engineering interest, consisting of a 3D thick rubber docks bumper and an extruded (2D) wheatear strip have been illustrated, using different mixtures (50–50%, 25–75% and 75–25%) of two peroxides.

Numerical simulations have shown how different mixtures of peroxides may (a) reduce optimal curing time at almost constant optimized tensile strength or (b) increase optimal tensile strength with an acceptable increase of the curing time.

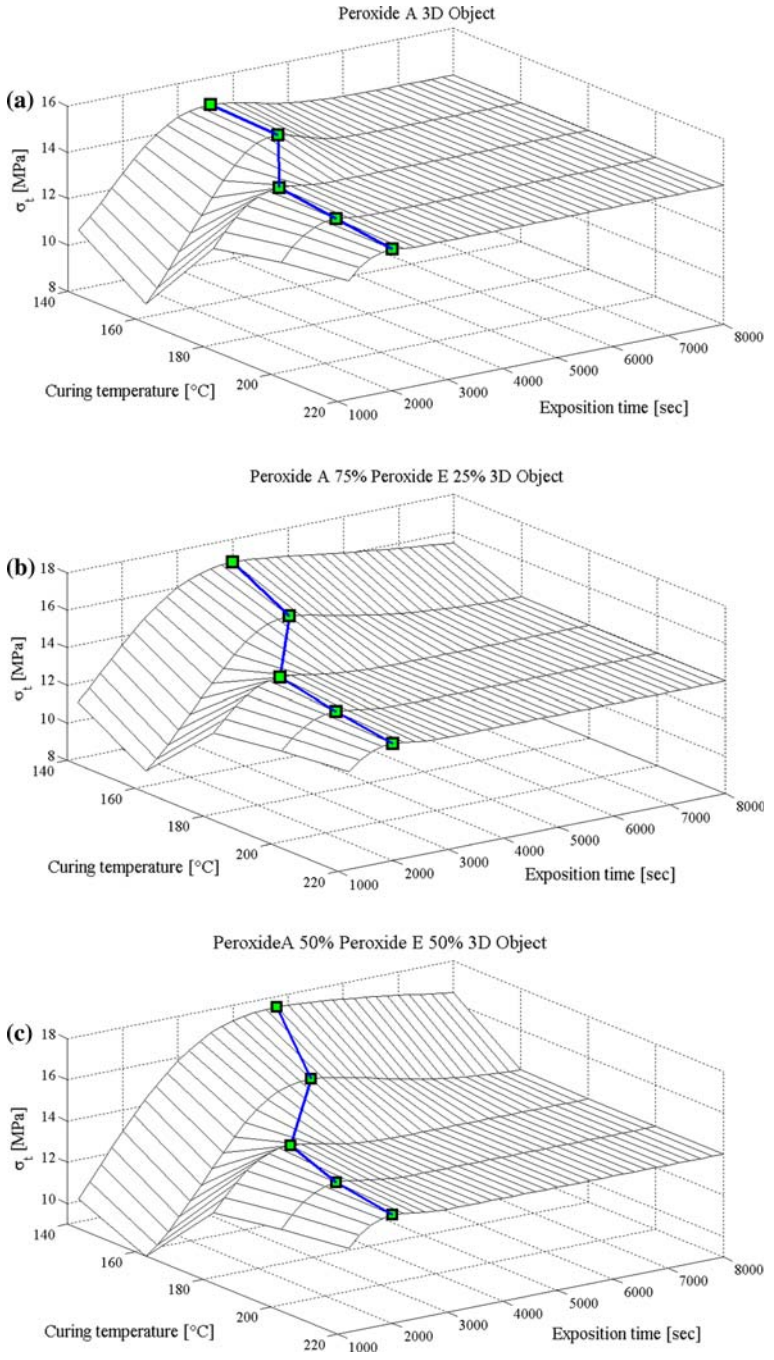

Fig. 24 Resultant tensile strength at different curing times, 3D object, 3D representation. **a** Peroxide A only. **b** 75% Peroxide A 25% Peroxide E. **c** 50% Peroxide A 50% Peroxide E. *Squares* refer to GA optimized resultant tensile strengths

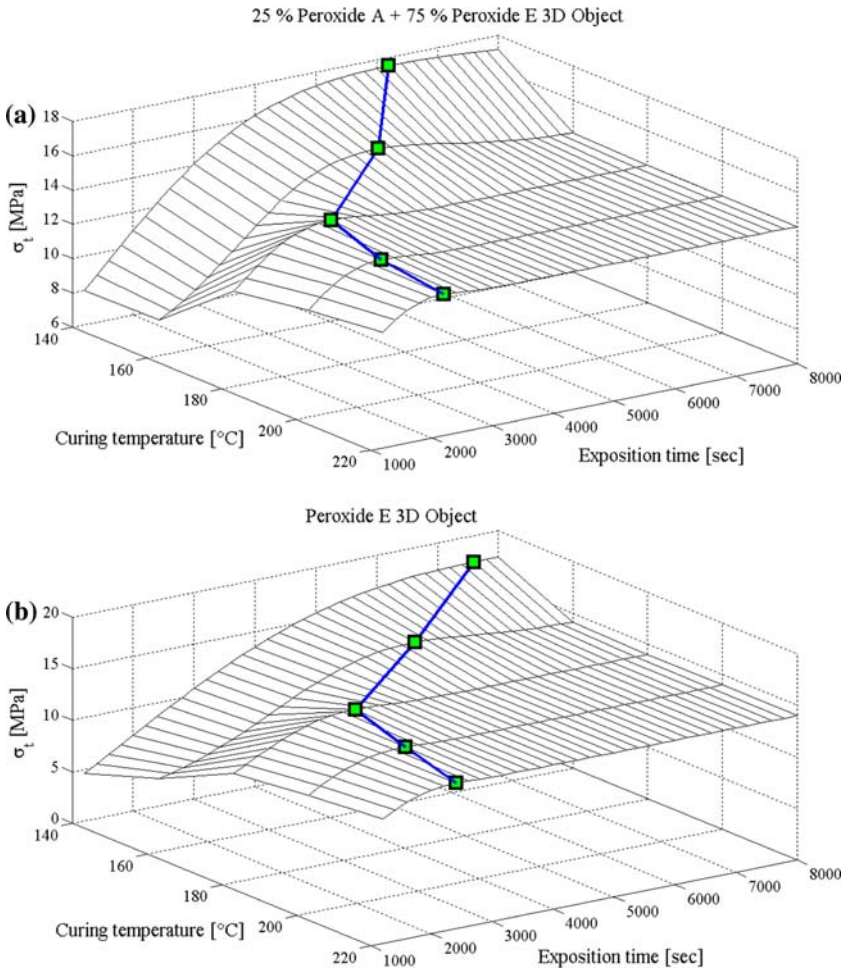

Fig. 25 Resultant tensile strength at different curing times, 3D object, 3D representation. **a** 25% Peroxide A 75% Peroxide E. **b** Peroxide E only. *Squares* refer to GA optimized resultant tensile strengths

Therefore, the numerical procedure proposed may represent a valuable tool for practitioners to obtain high quality level vulcanized items, limiting total curing time required.

References

1. D.C. Seymour, D. Krick, J. Elast. Plast. **11**, 97–109 (1979)
2. V. Kosar, Z. Gomzi, Thermochimica Acta **457**, 70–82 (2007)
3. V. Kosar, Z. Gomzi, K. Sintic, Chem. Eng. Process **46**(2), 83–88 (2007)
4. AkzoNobel Corporate. Brands and products specifications manual (2008)
5. L. Bateman (ed.), *The Chemistry and Physics of Rubber-like Substances* (MacLaren, London, 1963)
6. W. Hofmann, Kautschuk Gummi Kunststoffe, Jahrganf **4**, (1987)

7. A.Y. Coran, in *Vulcanization* (Chapter 7), ed. by R. Frederick Eirich Science and Technology of Rubber (Academic Press, New York, 1978)
8. M. Morton (ed.), *Rubber Technology*, 2nd edn. (Van Nostrand Reinhold, New York, 1981)
9. R.E. Drake, J.M. Labriola, J.J. Holliday, *Improving Properties of EPM and EPDM with Coagents* (American Chemical Society, Chicago, 1994)
10. R.E. Drake, J.M. Labriola, J.J. Holliday, *1,2 Polybutadiene Coagents for Improved Elastomeric Properties* (American Chemical Society, Nashville, 1992)
11. B.E. Roberts, S. Verne, Plastic Rubber Process Appl. **4**, 135 (1984)
12. E. Di Giulio, Ballini G., Kautschuk Gummi Kunststoffe 15(6) (1962)
13. J. Liu, W. Yu, C. Zhao, C. Zhou, Polymer **48**, 2882–2891 (2007)
14. J.A. Brydson, *Rubbery Materials and their Compounds* (Elsevier, Essex, 1988)
15. A.F. Trotman-Dickinson, J. Chem. Educ. **46**(6), 396–397 (1969)
16. J. Scanlan, D.K. Thomas, J. Polym. Sci. Part A **1**(3), 1015–1023 (1963)
17. F.P. Baldwin, G. Ver Strate, Rubber Chem. Technol. **45**, 709 (1972)
18. H.F. Mark, N.G. Gaylord, N.M. Bikales (eds.), *Encyclopaedia of polymer science and technology*, vol. 4 (Wiley-Interscience, New York, 1996), p. 332
19. L.D. Loan, Rubber Chem. Technol. **40**, 149 (1967)
20. W.C. Endstra, Kautschuk Gummi Kunststoffe **32**, 756 (1979)
21. R.H. Schwarr, C.H. Chien, Ethylene-Propylene co and ter polymer rubber. Report 4b, Stanford Research Institute: Menlo Park, CA (1981)
22. J.R. Dormand, P.J. Prince, J. Comp. Appl. Math. **6**, 19–26 (1980)
23. O.C. Zienkiewicz, R.L. Taylor, *The Finite Element Method, vol. I. Basic Formulations and Linear Problems* (McGraw-Hill, London, 1989)
24. ASTM D412. Standard test methods for vulcanized rubber and thermoplastic elastomers-tension
25. F.W. Billmeier Jr., *Textbook of Polymer Science*, 3rd edn. (Wiley, New York, Chichester, Brisbane, Toronto, Singapore, 1984)
26. G. Evans, J. Blackledge, P. Yardley, *Numerical Methods for Partial Differential Equations*, 2nd edn. (Springer, Berlin, 2001)
27. Y. Jia, S. Sun, S. Xue, L. Liu, G. Zhao, Polymer **44**, 319–326 (2003)
28. Y. Jia, S. Sun, S. Xue, L. Liu, G. Zhao, Polymer **43**, 7515–7520 (2002)
29. Matlab User's Guide 2007. http://www.mathworks.com/products/matlab/
30. D.E. Goldberg, *Genetic Algorithms in Search, Optimization and Machine Learning* (Addison Wesley, Reading, Massachusetts, 1989)
31. R.B. Holstien, Artificial genetic adaptation in computer control systems. Ph.D. Thesis. Department of Computer and Communication Sciences, University of Michigan, Ann Arbor (1971)
32. R.L. Haupt, S.E. Haupt, *Practical Genetic Algorithms* (Wiley, London, 2004)
33. Y. He, C.-W. Hui, Genetic algorithm based on heuristic rules for high-constrained large-size single-stage multi-product scheduling with parallel units. Chem. Eng. Process **43**(11), 1175–1191 (2007)
34. L. Montastruc, C. Azzaro-Pantel, L. Pibouleau, S. Domenech, Use of genetic algorithms and gradient based optimization techniques for calcium phosphate precipitation. Chem. Eng. Process. **43**(10), 1289–1298 (2004)
35. Y.-D. Kwon, S.-B. Kwon, S.-B. Jin, J.-Y. Kim, Convergence enhanced genetic algorithm with successive zooming method for solving continuous optimization problems. Comput. Struct. **81**, 1715–1725 (2003)
36. K.S. Lee, Z.W. Geem, A new structural optimization method based on the harmony search algorithm. Comput. Struct. **82**, 781–798 (2004)